Appendix A

Supplementary Information for Chapter 2

Adapted from:

Zott, M. D.; Canestraight, V. M.; Peters, J. C.
ACS Catal. **2022**, *12*, 10781–10786.
DOI: 10.1021/acscatal.2c03215.

.

A.1 General procedures

General Considerations: All manipulations were carried out using standard Schlenk or glovebox techniques under an N_2 or Ar atmosphere. Unless otherwise noted, solvents were deoxygenated and dried by thoroughly sparging with N_2 gas followed by passage through an activated alumina column in a solvent purification system (SG Water, USA LLC). All solvents were stored over activated 3 or 4 Å molecular sieves prior to use. Electrolytes were dried by heating (>100 °C) under vacuum (<1 torr) for at least 12 hours. All reagents were purchased from commercial vendors and used without further purification unless otherwise stated. [Cu_2] (also known as [(PNP$^{t\text{Bu}}$)Cu]$_2$) and its constituent protonated ligand (H-PNP$^{t\text{Bu}}$) were prepared as previously described.[1] ^{1}H NMR chemical shifts are reported in ppm relative to tetramethylsilane, using residual solvent resonances as internal standards.

Electrochemistry: Voltammetry experiments were carried out with a Biologic VSP or CH Instruments 600B potentiostat using a one-compartment three-electrode cell, and coulometry experiments were carried out with a Biologic VSP potentiostat using a two-compartment three-electrode cell. For voltammetry, a glassy carbon (GC) working electrode (3 mm diameter), a Pt wire counter electrode, and a Ag/AgOTf reference electrode (5 mM AgOTf and 0.2 M $LiNTf_2$ in DME) were employed. For CPC, the same reference electrode was used, but a carbon cloth (geometric area: 5 cm^2) and a Mg coil were used respectively as working and counter electrode. All redox potentials in the present work are reported versus SCE. Redox potentials were calibrated against Fc/Fc$^+$ and converted to SCE using $E_{SCE} = E_{Fc/Fc+} + 0.51$ V (Equation A1).[2]

CVs were collected at 100 $mV \cdot s^{-1}$ unless specified otherwise. $E_{1/2}$ values for the reversible waves were obtained from the half potential between the oxidative and reductive peaks. Irreversible waves have potentials reported as their peak potential (E_p).

NMR: NMR spectroscopy was performed using Varian and Bruker 400 or 600 MHz NMR spectrometers equipped with broadband auto-tune probes. ^{1}H NMR chemical shifts are reported in ppm relative to tetramethylsilane, using residual solvent resonances as internal standards.

UV-Vis: Spectra were collected using a Cary 60 instrument with Cary WinUV software. Spectra were background corrected.

Mass Spectrometry: Mass spectra were obtained in direct infusion mode with electrospray ionization on a Thermo Fisher LTQ Linear Ion Trap Mass Spectrometer. Ions were measured in the range 150–2000 m/z, and product ions were isolated and further analyzed by collision-induced dissociation to further corroborate identification.

X-ray Crystallography: XRD studies were carried out at the Beckman Institute Crystallography Facility on a Bruker D8 Venture diffractometer (Cu Kα radiation). Structures were solved using direct methods with SHELXS or SHELXT and refined against F^2 on all data by full-matrix least squares with SHELXL.[3] All of the solutions were performed in the Olex2 program.[4] The crystals were mounted on a glass fiber under Paratone N oil.

Luminescence: Steady-state and time-resolved luminescence measurements were carried out in the Beckman Institute Laser Resource Center at Caltech and performed under an Ar

atmosphere at room temperature. Samples were prepared in 1 cm path length quartz cuvettes in a dark, argon-filled glovebox. Prior to measurement, all samples were protected from light by wrapping in aluminum foil.

Steady-state emission spectra were recorded on a modified Jobin Yvon Spex Fluorolog-3. A xenon arc lamp was used for sample excitation, with wavelength selection performed by a monochromator. Luminescence was collected at 90° to the excitation direction and directed by a bifurcated optical fiber bundle to two Ocean Optics QEPro CCD spectrometers spanning 300 to 930 nm. Spectra were corrected for instrument response.

For time-resolved measurements, laser excitation was provided by 8 ns pulses from a Q-switched Nd:YAG laser (Spectra-Physics Quanta-Ray PRO-Series) operating at 10 Hz. The first harmonic was used to provide laser pulses at 355 nm. Probe wavelengths were selected for detection by a double monochromator (Instruments SA DH-10) with 1 mm slits. All instruments and electronics in these systems were controlled by software written in LabVIEW (National Instruments). Luminescence decay traces were fit to a single exponential (after an appropriate time delay to remove scattered excitation light).

For each Stern-Volmer series, 5 cuvettes were prepared with 20 μM [Cu_2] and quencher (40-320 μM) in DME in a dark argon glovebox. The cuvettes were sealed with a threaded Teflon valve and covered in aluminum foil to prevent ambient light exposure. Fluorescence lifetime measurements were carried out with excitation wavelength of λ_{ex} = 355 nm and a recording wavelength of λ_{em} = 510 nm at 25 °C. A long pass filter λ>500 was used to diminish scattered excitation light. The emission decay was averaged over 50 laser

pulses and was fit to a monoexponential function. The lifetime was determined to occur when the intensity was 1/e its initial value, or I_0/e.

Chromatography: All chromatography experiments were performed using standard silica gel unless otherwise indicated. For column chromatography, F60, 40 – 63 μm, 60 Å silica from SiliCycle (R10030B) was used. For thin layer chromatography, aluminum-backed 60 Å silica gel coated with a 254 nm fluorescent indicator was used (MilliporeSigma, EM1.05554.0001).

A.2 Luminescence data for [Cu_2]

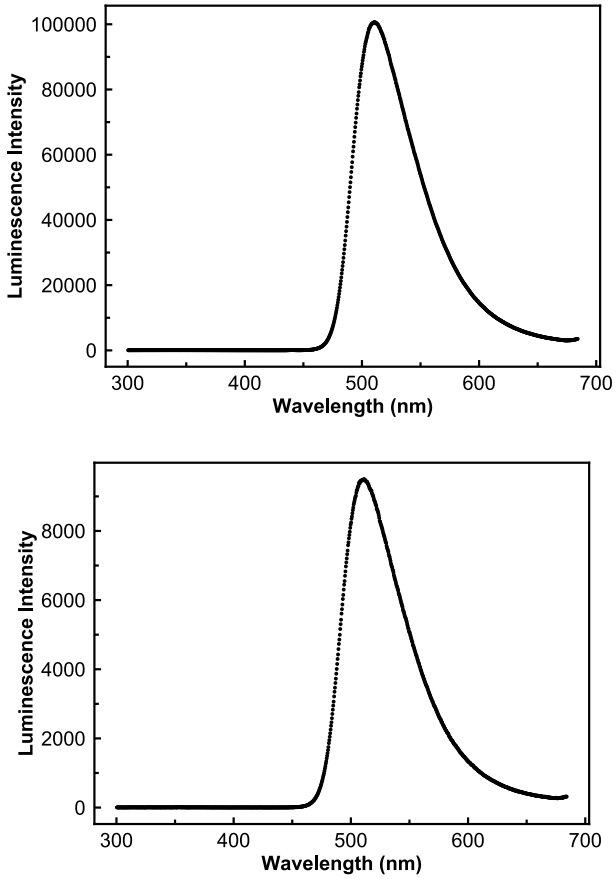

Figure A1. Emission spectra for 160 μM [Cu_2] in DME with excitation at 440 nm (left) or 355 nm (right).

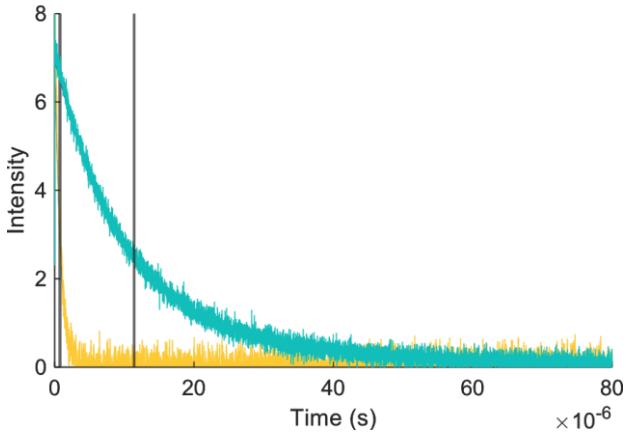

Figure A2. Example time-resolved luminescence decays for 20 µM [Cu_2] in DME with excitation at 355 nm. The teal trace has no additives; the yellow trace is in the presence of a quencher, 160 µM 4-cyanobenzyl chloride. Gray vertical lines are plotted at the timepoint at which the luminescence intensity is reduced to 1/*e* of the initial value, representing the lifetime (τ).

A.3 Stern-Volmer plots and Marcus theory analysis

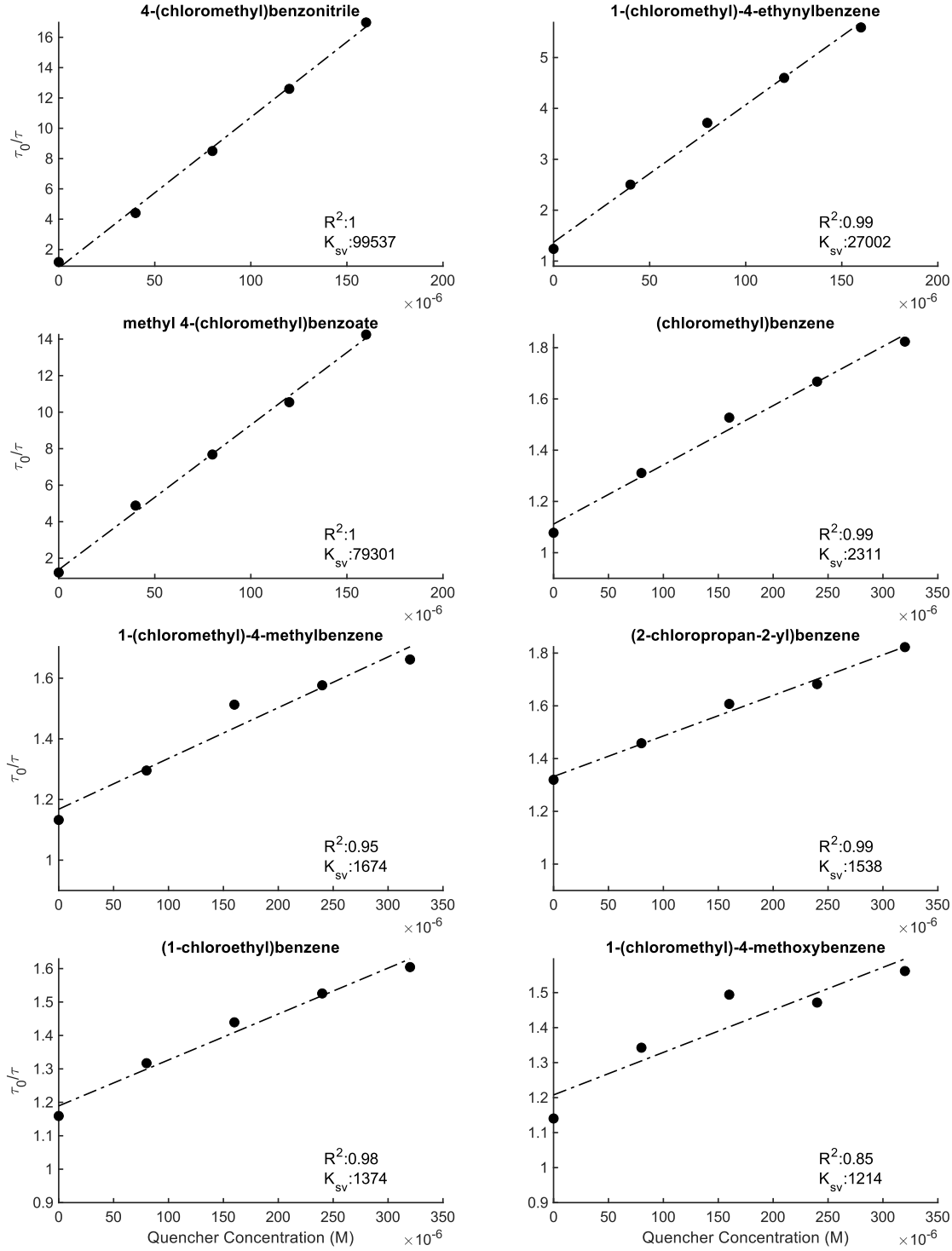

Figure A3. Stern-Volmer plots of 20 μM [Cu_2] in DME in the presence of various benzyl chloride quenchers at 25 °C. This data is presented in the main text as one plot with all eight SV plots overlaid.

Based on these quenching rates and the driving force as estimated using various redox potential data for the benzyl chloride quenchers, an analysis following Marcus theory was performed. Using non-linear regression (Levenberg–Marquardt) and the simplified Marcus equation (Equation A2) for transfer between neutral molecules,[5] relating k_{obs} and ΔG (defined as K_{SV}/τ_0 and $E_{quencher}-E_{ox}^{*}$, respectively), the reorganization energy (λ) was obtained and compared using $E_{quencher}$ values from: peak potentials (E_p), half-peak potentials ($E_{p/2}$), and potentials from differential pulse voltammetry (DPV).

$$\ln(k_{obs}) = -\left[\frac{\lambda}{4RT}\left(1+\frac{\Delta G}{\lambda}\right)^2\right] + \text{Const.} \qquad \text{(Equation A2)}$$

The data using peak potentials is presented in the main text, but all data sets yield qualitatively identical results. All fits are presented below. These various $E_{quencher}$ values result in different reorganization energies in the range: λ = 18.8–37.1 kcal/mol, which are low to modest in magnitude. Using E_p data to model driving force better reproduces the low driving force regime, whereas using DPV data better reproduces the high driving force regime. The deviations at high driving force for the E_p data set could result from nearing the diffusion limit, a challenge first discussed by Rehm and Weller, whereupon the inverted region is not observed in certain photoinduced charge transfer reactions.[6]

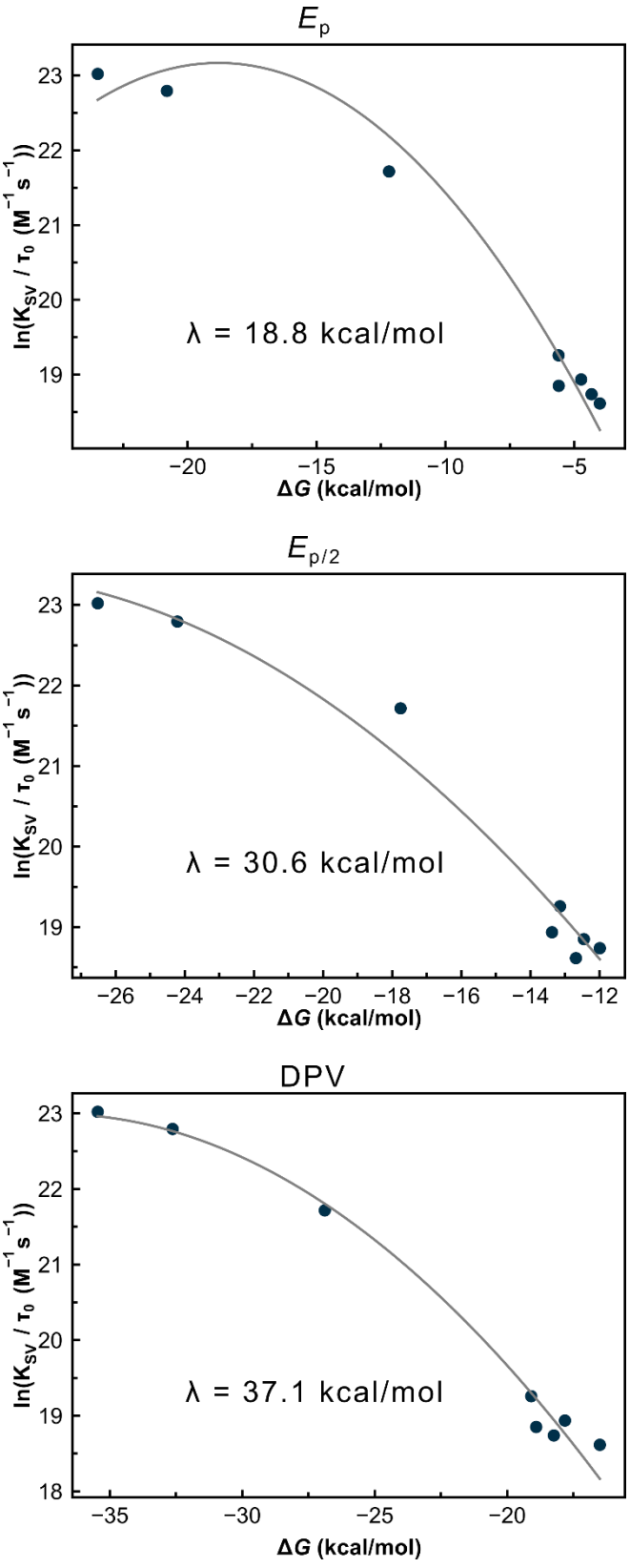

Figure A4. Rate-driving force relationships modelled using Marcus theory at T = 25 °C.

A.4 Cyclic voltammograms of benzyl chloride quenchers

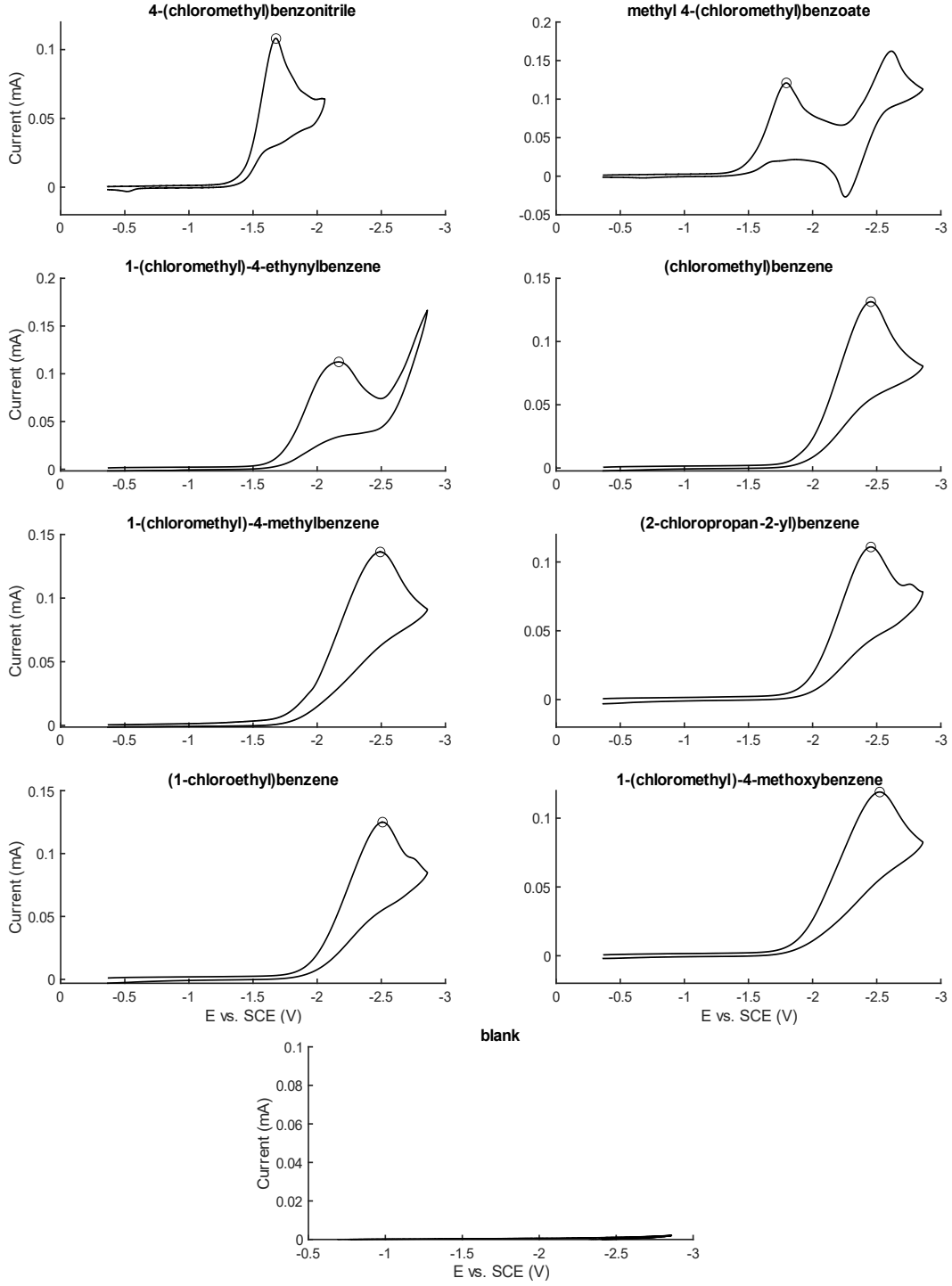

Figure A5. Cyclic voltammograms of various benzyl chlorides**.** Recorded in DME with 5 mM benzyl chloride and 0.2 M $TBAPF_6$. Glassy carbon working electrode, Ag/AgOTf reference electrode, and Pt counter electrode. Scan rate: 100 mV/s.

Note that these cyclic voltammograms were recorded in DME with $TBAPF_6$ supporting electrolyte instead of $LiNTf_2$, the optimum electrolyte for controlled potential coulometry. Unfortunately, the solvent window with 0.2 M $LiNTf_2$ was too narrow and thus the benzyl chloride reduction waves were masked.

A.5 UV-vis time-course data

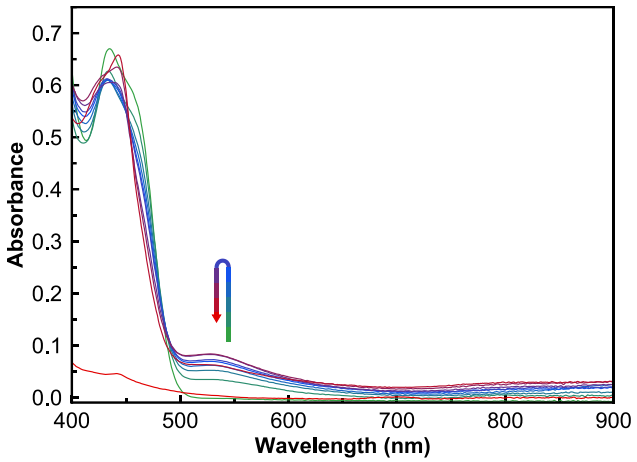

Figure A6. UV-vis spectra of 160 µM [Cu_2] in DME taken after 440 nm irradiation for 0, 1, 2, 3, 4, 5, 10, 15, 30, and 300 cumulative seconds. The colors change from greens (0–3 s) to blues (4–10 s) to reds (15–300 s). A subset of this data is presented in the main text.

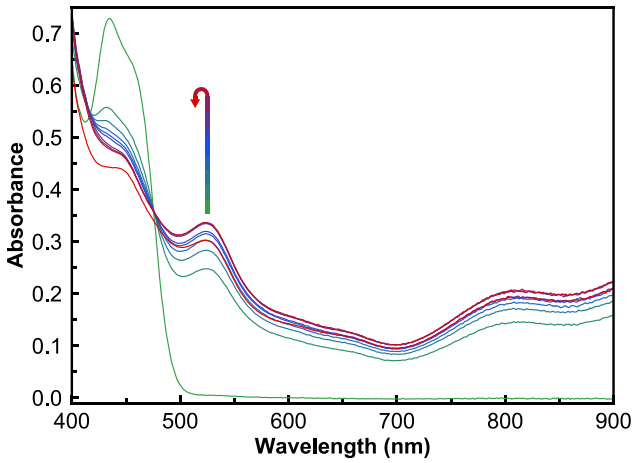

Figure A7. UV-vis spectra of 160 µM [Cu_2] in DME with 0.2 M $LiNTf_2$ taken after 440 nm irradiation for 0, 1, 2, 3, 4, 5, 10, 15, 30, and 300 cumulative seconds. The colors change from greens (0–3 s) to blues (4–10 s) to reds (15–300 s). A subset of this data is presented in the main text.

A.6 Synthesis and characterization of chloro-cubane and chloro-diamond

Chloro-cubane, $[(H\text{-}PNP^{tBu})Cu_2Cl_2]_2$

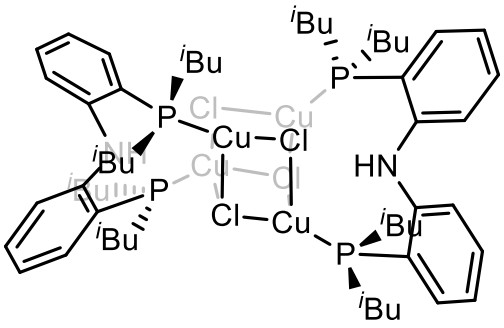

In a glovebox, H-PNP^{tBu} (50 mg, 1 eq) and copper(I) chloride (17.4 mg, 2 eq) were combined in tetrahydrofuran (1 mL) and stirred for 1 day. The solution remained colorless. The solution was concentrated and triturated with pentane prior to being dissolved in pentane:tetrahydrofuran (2 mL, 9:1) and filtered through a glass microfilter. After concentration, the product was afforded as a white solid (Yield: 65.0 mg, 99%).

^{1}H NMR (C_6D_6, 400 MHz): δ (ppm) = 7.93 (s, 1H), 7.55 (d, J = 8.3 Hz, 2H), 7.14 – 7.08 (m, 4H), 2.83 – 1.68 (m, 12H), 1.33–0.72 (m, 42H).

^{31}P NMR (C_6D_6, 162 MHz): δ (ppm) = −28.5 (s).

MS (FD, *m/z*): $[M]^+$ calculated: 1530.44911, found: 1530.44884.

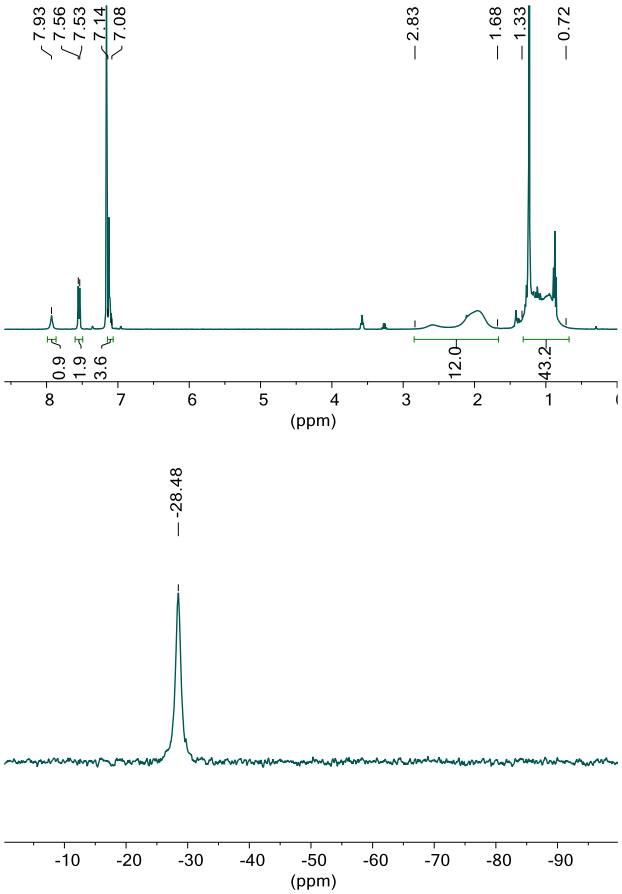

Figure A8. ^{1}H (left) and ^{31}P (right) NMR spectra for chloro-cubane in C_6D_6. The broadness of the peaks may be attributed to fluxionality in solution.

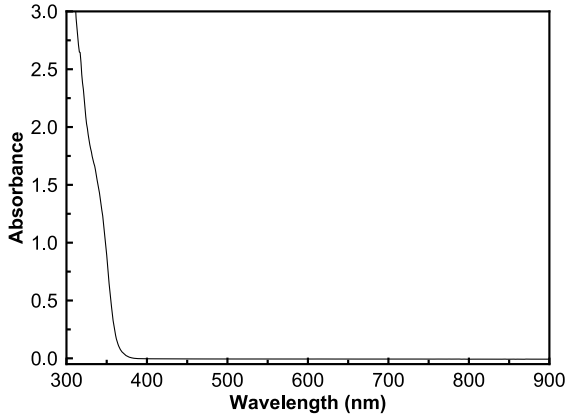

Figure A9. UV-vis absorption spectrum for 130 µM chloro-cubane in DME.

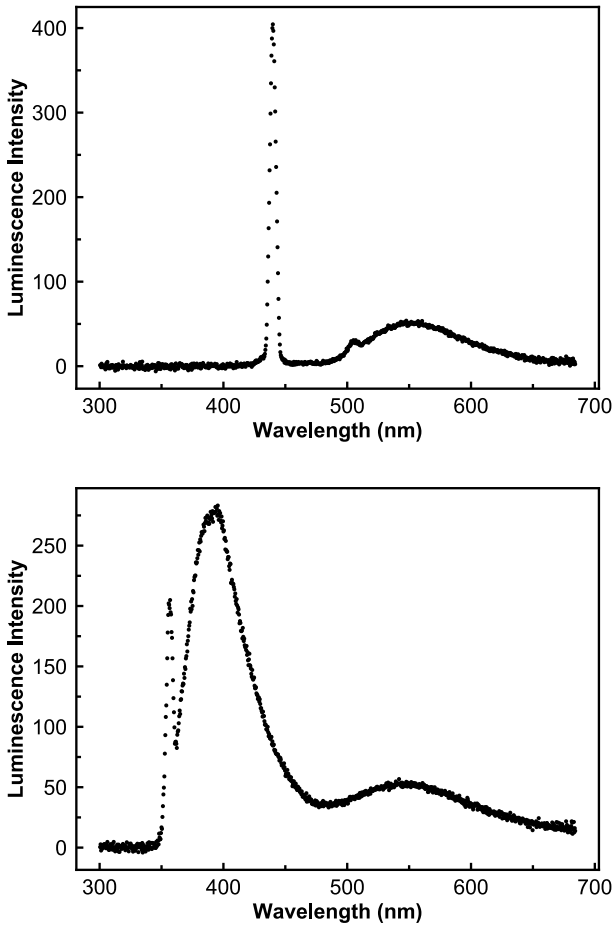

Figure A10. Emission spectra for 130 μM chloro-cubane in DME with excitation at 440 nm (left) or 355 nm (right).

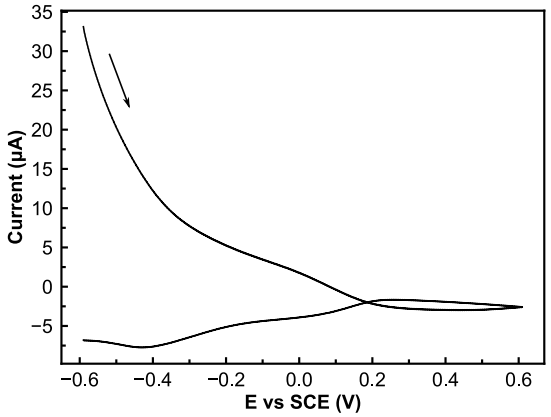

Figure A11. Cyclic voltammogram for ~1 mM chloro-cubane in DME with 0.2 M LiNTf2 supporting electrolyte, GC working, Pt counter, and Ag/AgOTf reference electrodes. Scan rate: 100 mV/s.

Chloro-diamond, [(H-PNP^{tBu})CuCl]$_2$

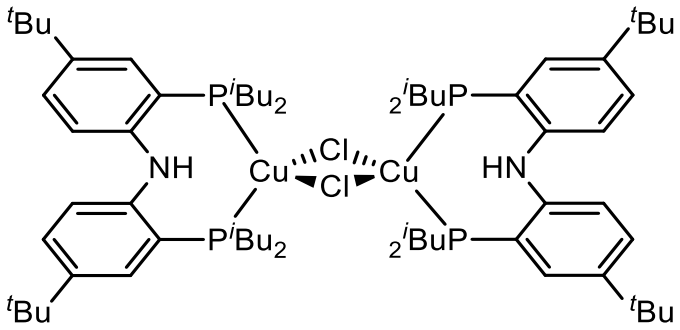

In a glovebox, H-PNP^{tBu} (50 mg, 1 eq) and copper(I) chloride (8.7 mg, 1 eq) were combined in tetrahydrofuran (1 mL) and stirred for 1 day. The solution remained colorless. The solution was concentrated and triturated with pentane prior to being dissolved in pentane:tetrahydrofuran (2 mL, 9:1) and filtered through a glass microfilter. After concentration, the product was afforded as a white solid (Yield: 56.1 mg, 96%).

^{1}H NMR (C_6D_6, 400 MHz): δ (ppm) = 10.96 (t, *J* = 11.1 Hz, 1H), 7.47 (q, *J* = 3.3 Hz, 2H), 7.42 (dt, *J* = 8.7, 2.6 Hz, 2H), 7.21 (dd, *J* = 8.6, 2.3 Hz, 2H), 2.06 (m, 8H), 1.80 – 1.64 (m, 4H), 1.11 (d, *J* = 6.3 Hz, 12H), 0.84 (d, *J* = 6.5 Hz, 12H).

^{31}P NMR (C_6D_6, 162 MHz): δ (ppm) = −42.5 (s).

MS (FD, *m/z*): $[M]^+$ calculated: 1334.65221, found: 1334.65070.

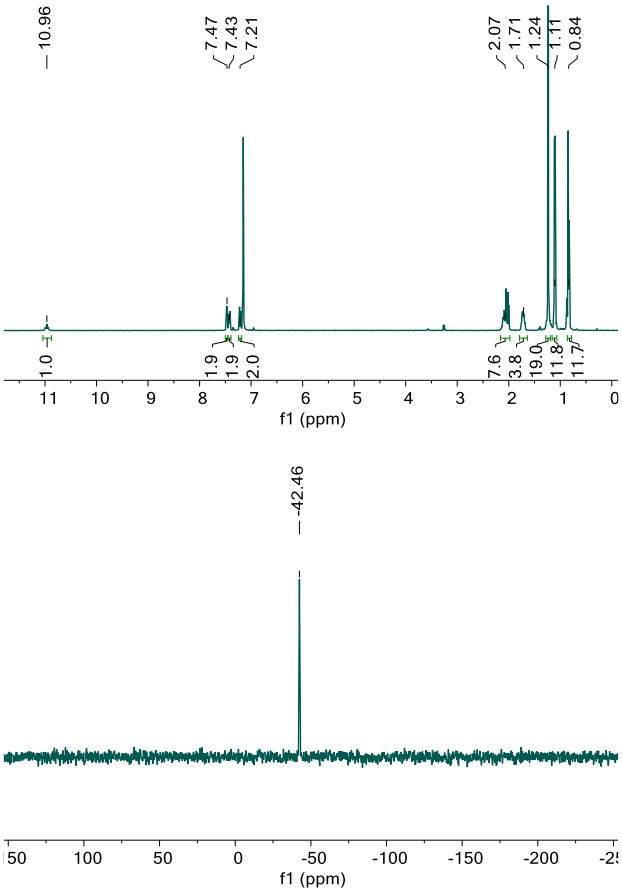

Figure A12. ^{1}H (left) and ^{31}P (right) NMR spectra for chloro-diamond in C_6D_6.

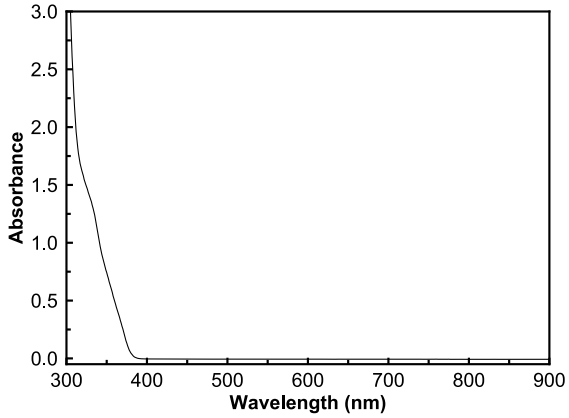

Figure A13. UV-vis absorption spectrum for 120 μM chloro-diamond in DME.

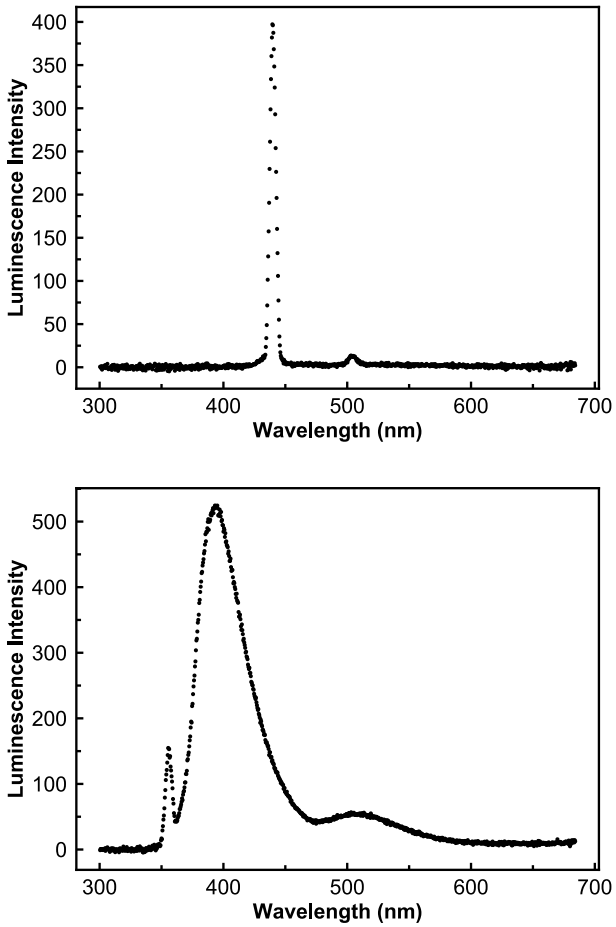

Figure A14. Emission spectra for 120 μM chloro-diamond in DME with excitation at 440 nm (left) or 355 nm (right).

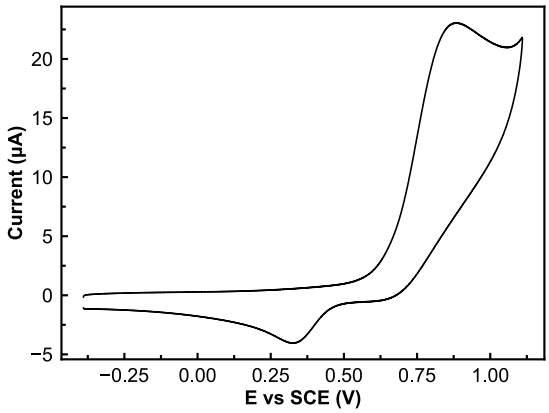

Figure A15. Cyclic voltammogram for ~1 mM chloro-diamond in DME with 0.2 M LiNTf2 supporting electrolyte, GC working, Pt counter, and Ag/AgOTf reference electrodes. Scan rate: 100 mV/s.

A.7 X-ray crystallography of chloro-cubane and chloro-diamond

The structures for chloro-cubane and chloro-diamond (see Figure 2 of maintext) were obtained in a single crystal containing each independent molecule. Due to the limited quality of the data obtained we do not provide detailed discussion of bond metrics. Still, the structures obtained corroborate their assignments and are of value to the discussion in the maintext.

Chloro-cubane and chloro-diamond crystallize together in the monoclinic space group $P2_1/c$ with one molecule each in the asymmetric unit. The structure was strongly disordered (see refinement details below). The program PLATON[7] revealed the presence of large voids which were not able to be refined, and the program SQUEEZE[8] was used to remove the contribution of the disordered electron density inside this void from the structure factors.

Whole molecule disorder was modeled for chloro-cubane. All non-hydrogen atoms were refined anisotropically. All hydrogen atoms were included into the model at geometrically calculated positions and refined using a riding model. Although hydrogen atoms bound to the diphenylamine nitrogens were not located in the difference map, their presence was experimentally corroborated by high-res mass spec and ^{1}H NMR. The isotropic displacement parameters of all hydrogen atoms were fixed to 1.2 times the *U* value of the atoms they are linked to (1.5 times for methyl groups). All disordered atoms were refined with the help of similarity restraints on the 1,2- and 1,3-distances. All atoms were refined with the help of similarity restraints on the displacement parameters as well as rigid bond restraints for anisotropic displacement parameters.

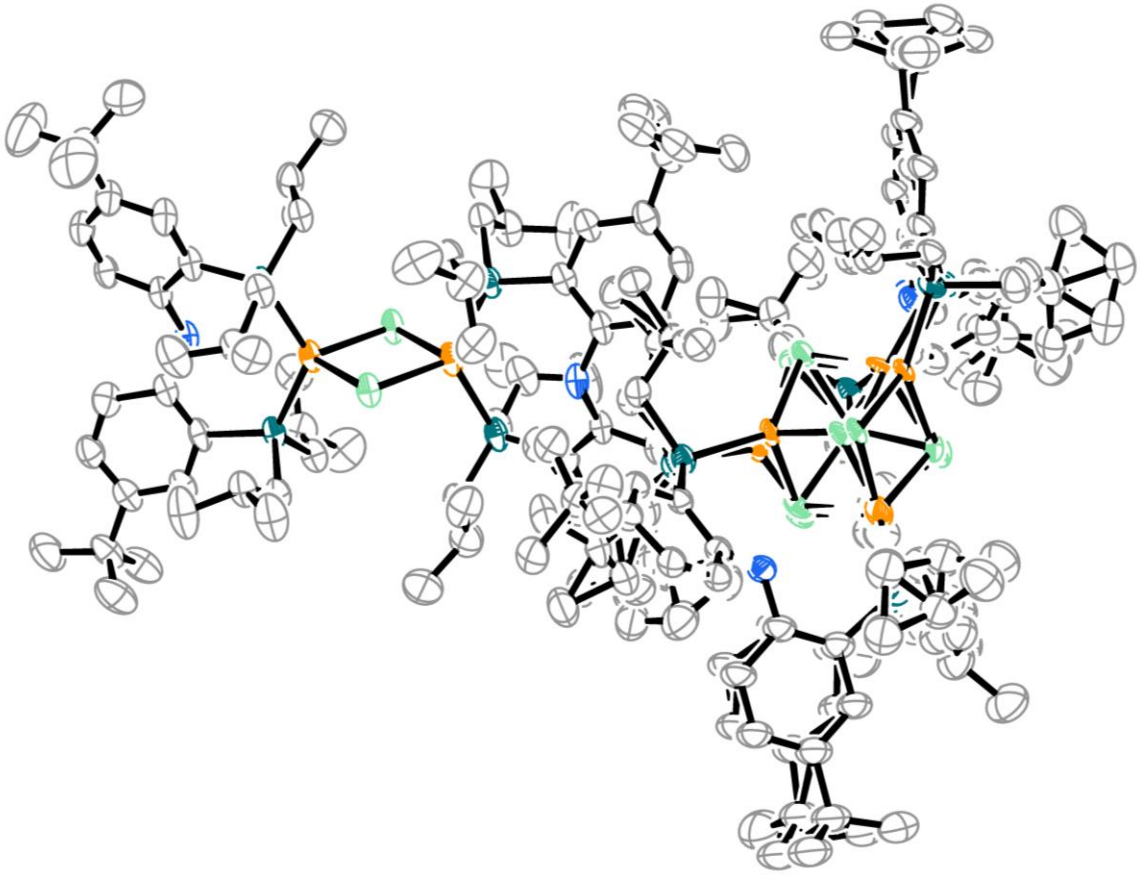

Figure A16. Solid-state structure of cocrystallized chloro-cubane and chloro-diamond with thermal ellipsoids shown at 50%. Hydrogen-atoms are not shown for clarity. The whole molecule disorder model for chloro-cubane is shown.

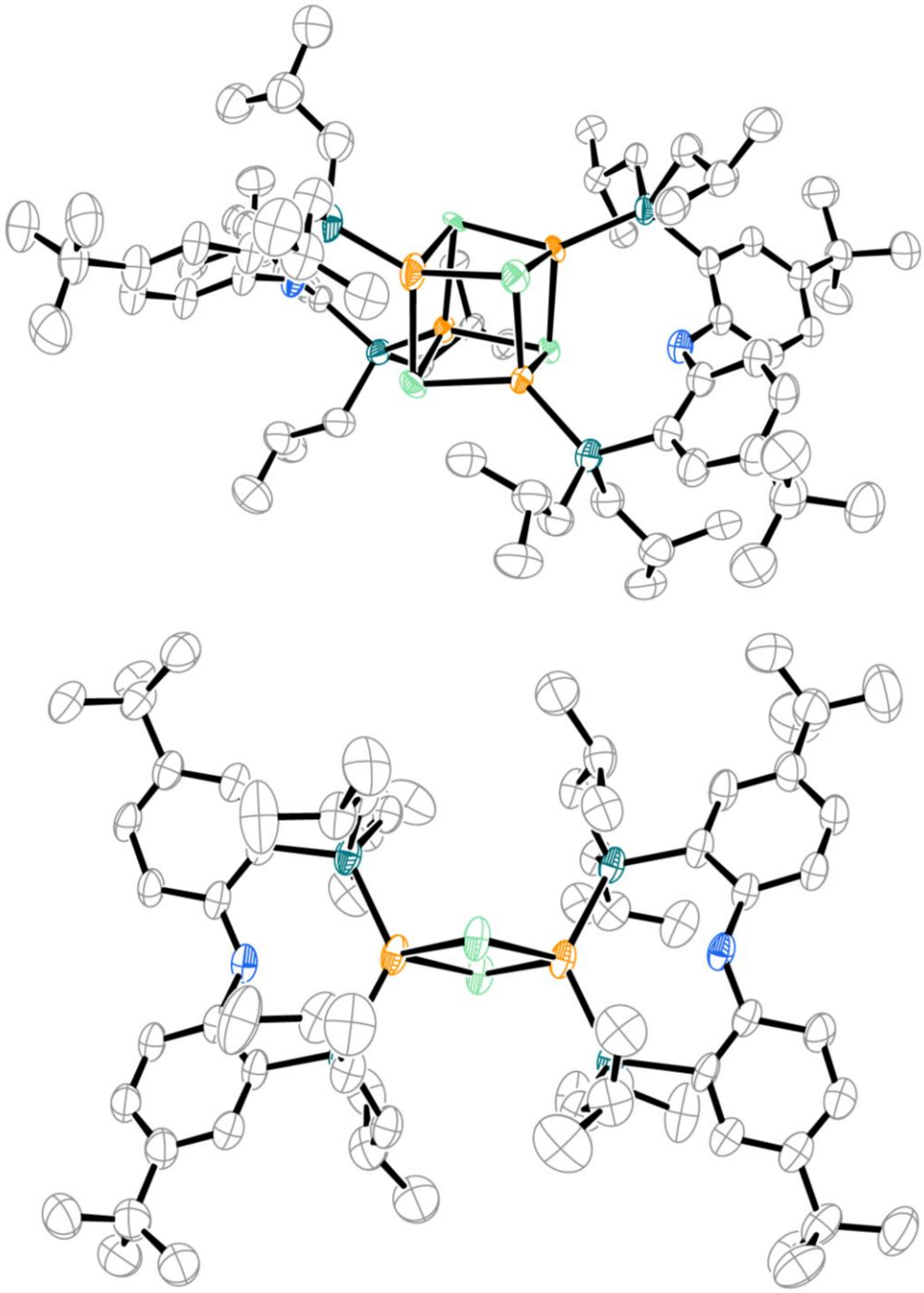

Figure A17. Solid-state structures of chloro-cubane (top) and chloro-diamond (bottom) extracted from the cocrystalline structure with thermal ellipsoids shown at 50%. Hydrogen-atoms are not shown for clarity. Only one of the two disordered sites is shown for chloro-cubane for clarity.

A.8 NMR and luminescence data of irradiated reaction mixtures

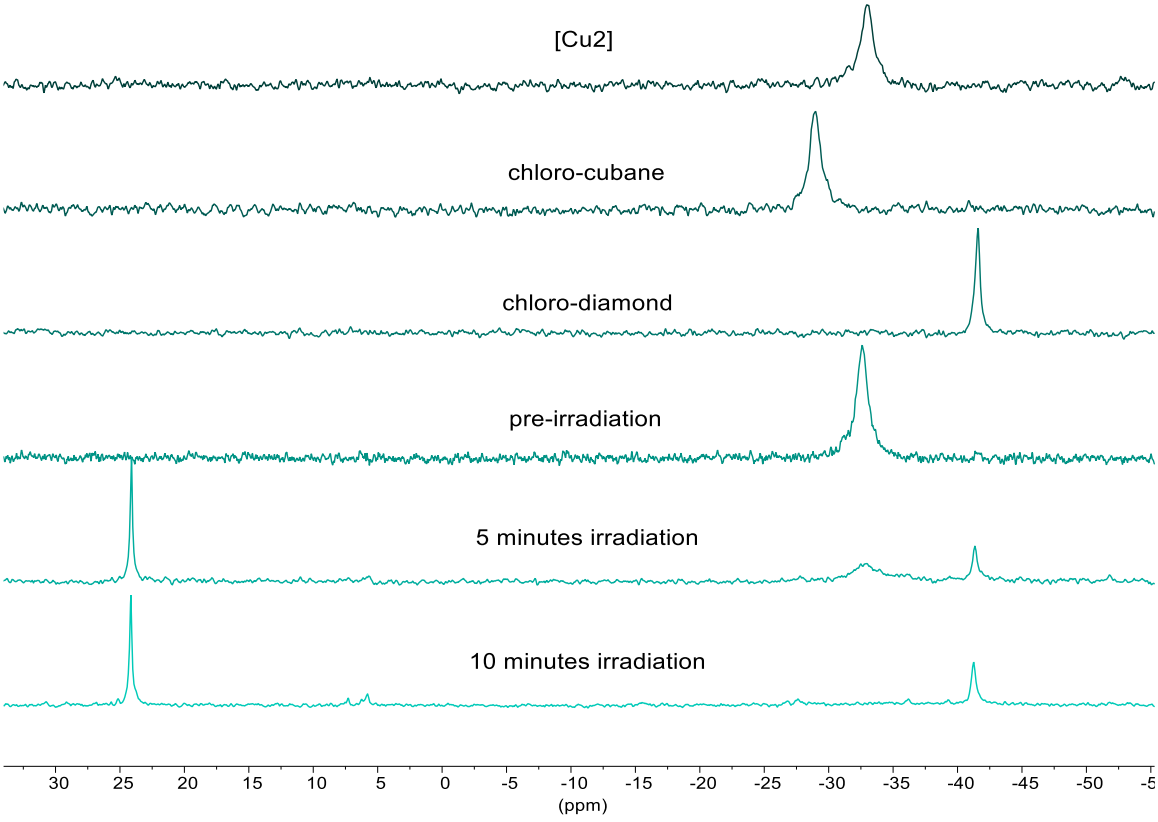

Figure A18. ^{31}P NMR spectra recorded in DME. The top three spectra are for isolated [Cu_2], chloro-cubane, and chloro-diamond. The bottom three spectra correspond to an NMR experiment containing [Cu_2] in the presence of 30 equivalents of 4-methylbenzyl chloride. Pre-irradiation, only starting material is observed. After 5 minutes of 440 nm irradiation, an unknown peak at 24.5 ppm, starting material, and chloro-diamond are observed. After 10 minutes, the unknown 24.5 ppm peak and chloro-diamond are the major phosphorus containing diamagnetic products.

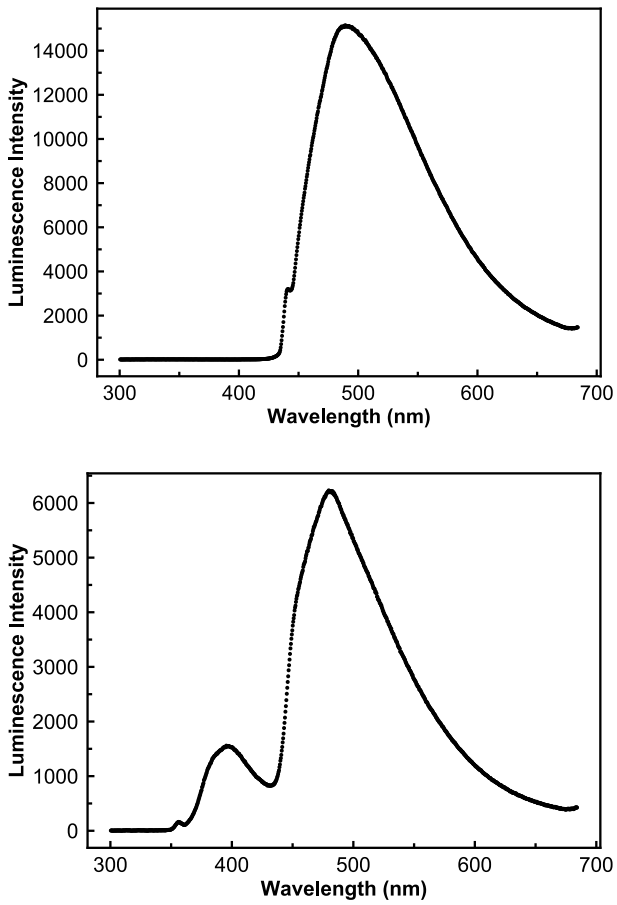

Figure A19. Emission spectra for a solution of 160 μM [Cu_2] in DME with 30 equivalents 4-methylbenzyl chloride after 440 nm irradiation for 5 minutes. Excitation was performed at 440 nm (left) or 355 nm (right).

A.9 Kinetics data for interaction of chloride and $[Cu_2]^+$

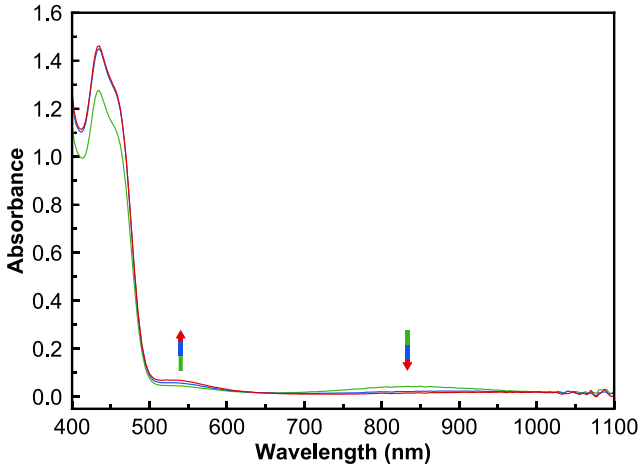

Figure A20. UV-vis traces for a mixture of $[Cu_2]^+$ (560 µM) and tetrabutylammonium chloride (5.6 mM, 10 eq) in DME at 30 s (green), 60 s (blue), and 90 s (red) at room temperature. Loss of $[Cu_2]^+$ absorbances is almost instantaneous upon mixing; thus, under these conditions, kinetics measurements were not possible due to the rapid rate of the reaction. Note that no change is observed over at least 1 hour for UV-vis spectra of $[Cu_2]^+$ in DME in the absence of tetrabutylammonium chloride.

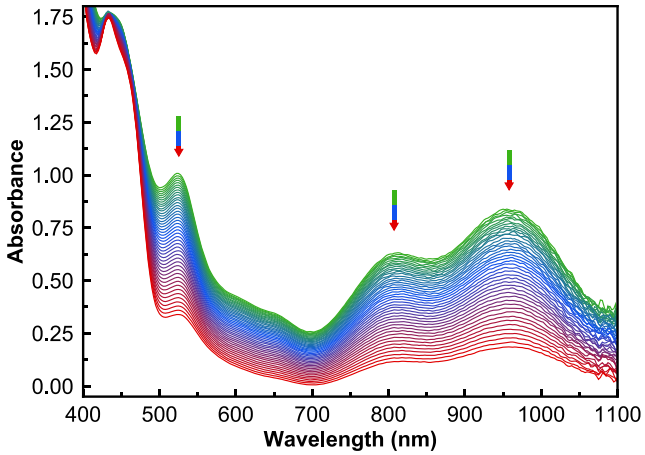

Figure A21. UV-vis traces for a mixture of $[Cu_2]^+$ (560 µM) and tetrabutylammonium chloride (5.6 mM, 10 eq) in DME with 0.2 M $LiNTf_2$ at 30 s intervals (green to blue to red) at room temperature.

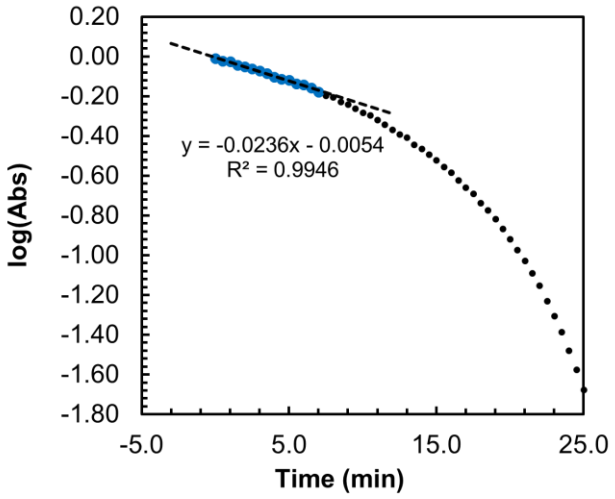

Figure A22. Kinetic trace monitoring absorbance at 958 nm versus time for a mixture of $[Cu_2]^+$ (560 µM) and tetrabutylammonium chloride (5.6 mM, 10 eq) in DME with 0.2 M $LiNTf_2$ at room temperature. The linear initial rate (highlighted as blue points) observed in the plot of log(Abs) versus time is characteristic of a first-order process.

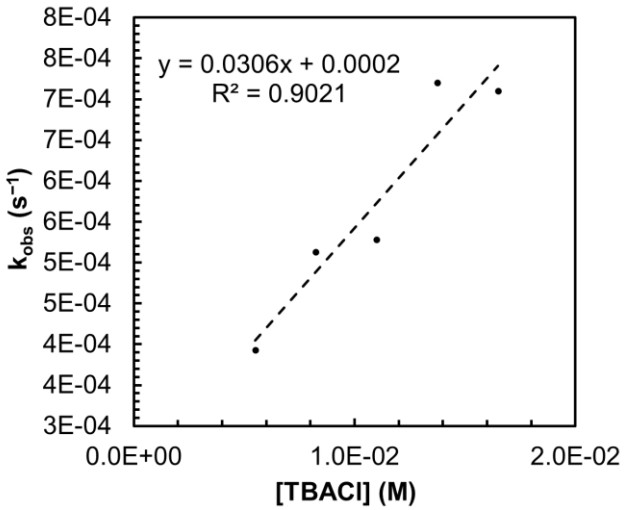

Figure A23. Analysis of the reaction rate for $[Cu_2]^+$ (560 µM) and tetrabutylammonium chloride (TBACl; 10–30 eq) in DME with 0.2 M $LiNTf_2$ at room temperature. A linear relationship between k_{obs} and TBACl concentration is observed.

A.10 Controlled potential coulometry procedures

General Procedure: In a glovebox, 4 mL of 1,2-dimethoxyethane solution containing lithium bis(trifluoromethane)sulfonimide electrolyte (0.2 M) is added to each side of an oven-dried two compartment (H-type) cell equipped with a fine porosity glass frit. The anode side is equipped with a coiled magnesium ribbon (3 mm x 0.2 mm x 5 cm) counter electrode. Prior to use, the magnesium electrode is rinsed with dilute (~1 M) HCl, water, and acetone. The 1,2-dimethoxyethane solution from the cathode side is used to transfer the benzyl chloride electrophile (0.15 mmol) and [Cu_2] photoredox catalyst (2.8 mg, 1.5 mol %) into the cathode compartment. The cathode compartment is fitted with a carbon cloth working electrode and Ag/AgOTf reference electrode.

The cell is removed from the glovebox, a nitrogen line is fitted, a fan is directed toward the cell, and the electrodes are connected to a potentiostat. The cell is polarized to a constant potential of −0.15 V vs SCE and a 440 nm Kessil lamp (Kessil PR160, intensity 50) placed 3 inches from the cathode compartment is turned on.

After ~1 h, a second portion of [Cu_2] photoredox catalyst (2.8 mg, 1.5 mol %) is transferred via syringe to the cell using an additional 0.2 mL of 1,2-dimethoxyethane solution containing lithium bis(trifluoromethane)sulfonimide electrolyte (0.2 M). This was found to increase yields by ~10% as compared to adding all of the catalyst in the beginning.

When the current decreases to ~5% of the initial current (1.5–3 hours), the lamp is turned off and the cell is disconnected from the potentiostat. The working and reference electrodes are removed from the cell and rinsed into the cell with 1,2-dimethoxyethane. The

solution from the cathode compartment is removed and concentrated on a rotary evaporator. Once concentrated, drying under high vacuum (<1 torr) is critical to reduce the 1,2-dimethoxyethane content as 1,2-dimethoxyethane can coordinate lithium bis(trifluoromethane)sulfonimide and facilitate its passage through chromatography media. This residue is dissolved in ethanol-free chloroform and eluted through a plug of neutral alumina to remove the lithium bis(trifluoromethane)sulfonimide electrolyte. Dichloromethane better solubilizes lithium bis(trifluoromethane)sulfonimide and should not be used. The eluant is concentrated and transferred to an NMR tube using $CDCl_3$. Dibromomethane (5 µL) is added as an internal standard, and a one-pulse ^1H qNMR spectrum is acquired.

Graphical Procedure:

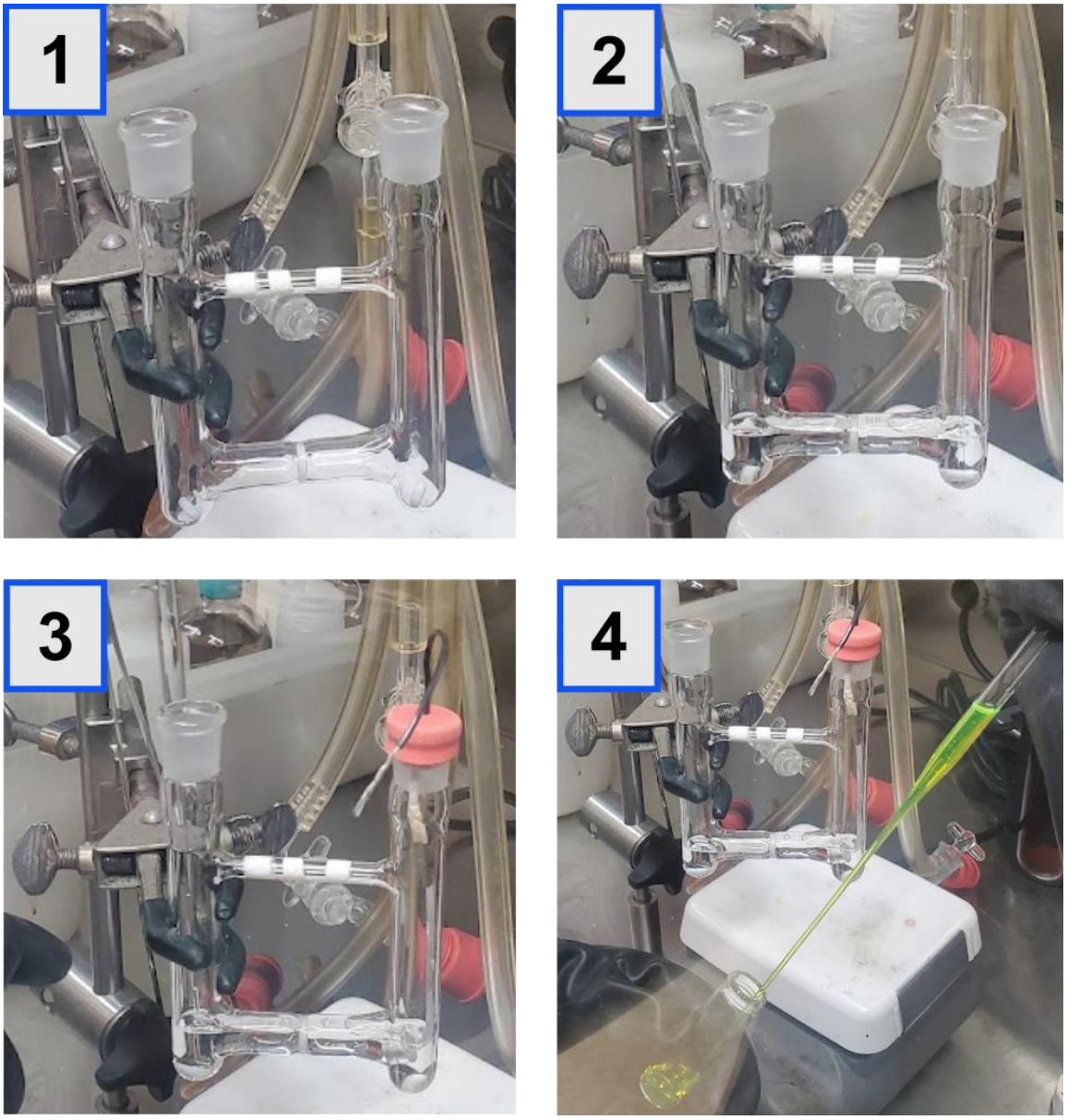

1. Place empty, oven-dried two compartment cell in glovebox.
2. Fill each compartment with 4 mL of 0.2 M $LiNTf_2$ in 1,2-dimethoxyethane (DME).
3. Fit counter electrode compartment with magnesium coil electrode.
4. Dissolve [Cu_2] in working electrode compartment using the DME electrolyte solution.

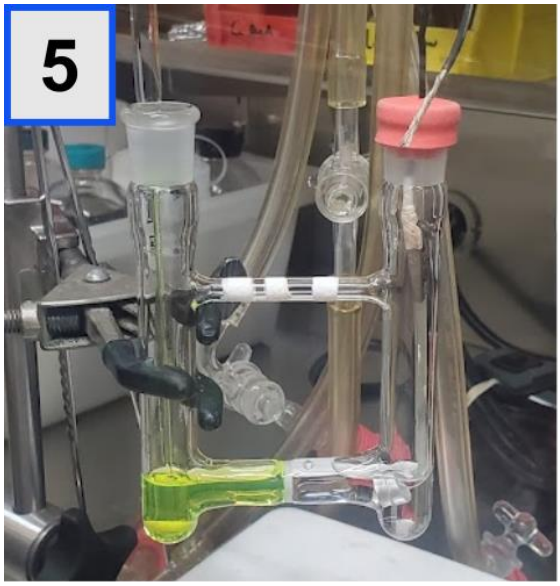

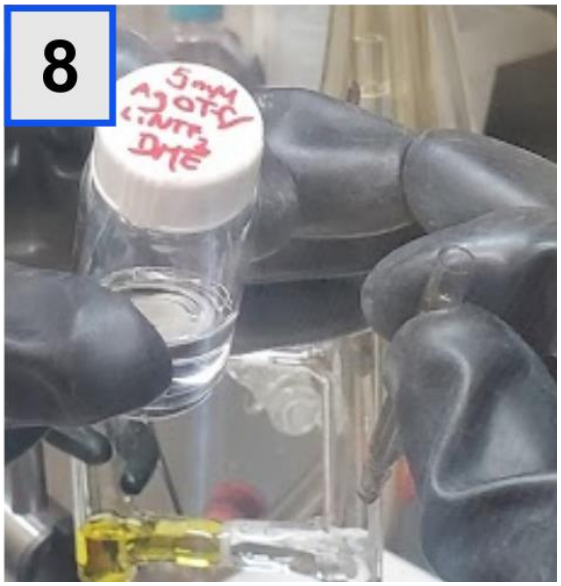

5. Transfer [Cu_2] solution into working electrode compartment.
   At this stage, the rest of the steps are performed with the lights off (lights left on here for clarity).

6. Dissolve benzyl chloride electrophile using working electrode compartment solution.

7. Transfer electrophile solution into working electrode compartment.

8. Fill reference electrode shell with 5 mM Ag^+ solution.

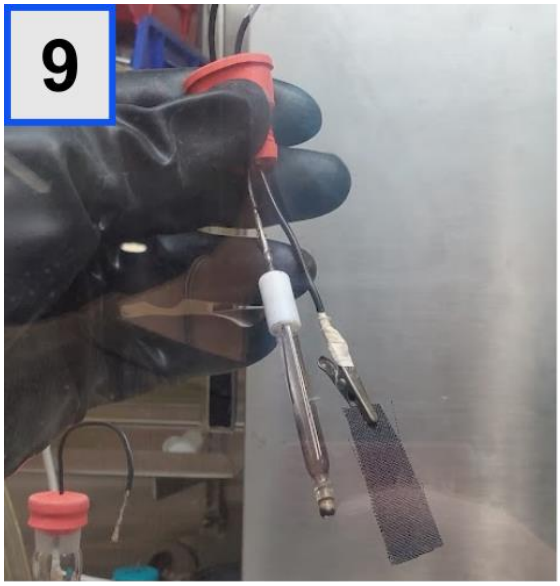

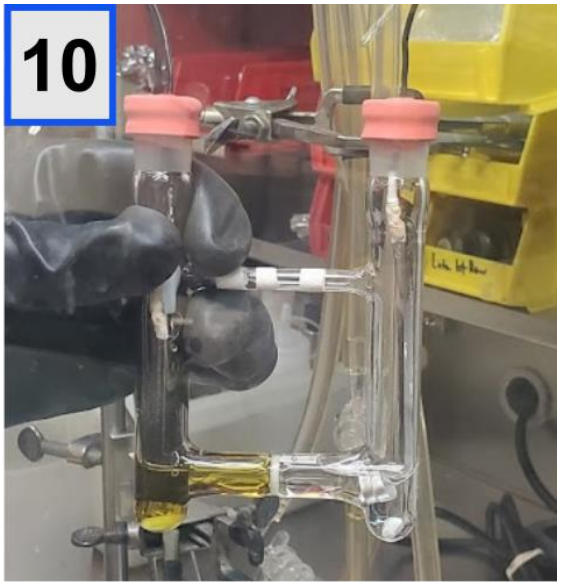

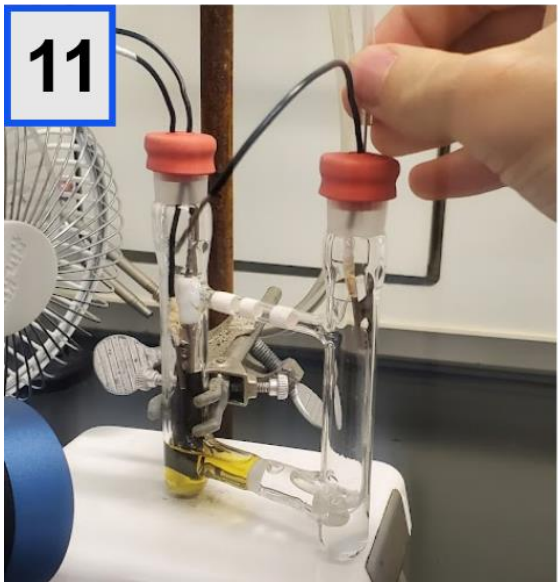

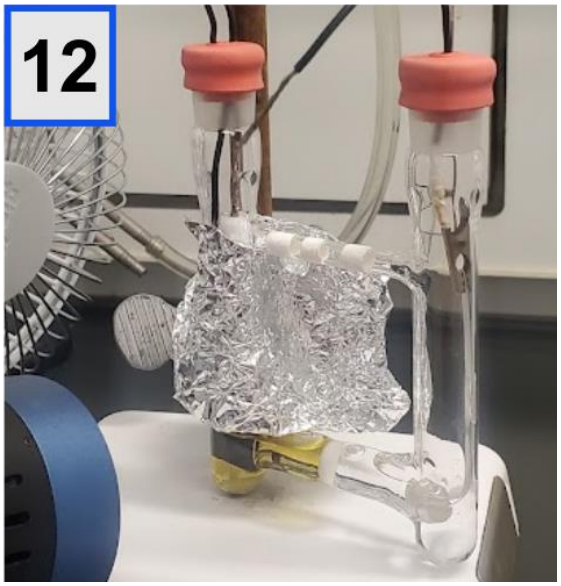

9. Fit reference electrode shell to wire cap; carbon cloth working electrode shown on right hand side.
10. Fit working and reference electrodes into working electrode compartment.
11. Remove cell from glovebox and insert nitrogen inlet through septum.
12. Protect upper part of reference electrode with aluminum foil (Ag^+ is light sensitive).

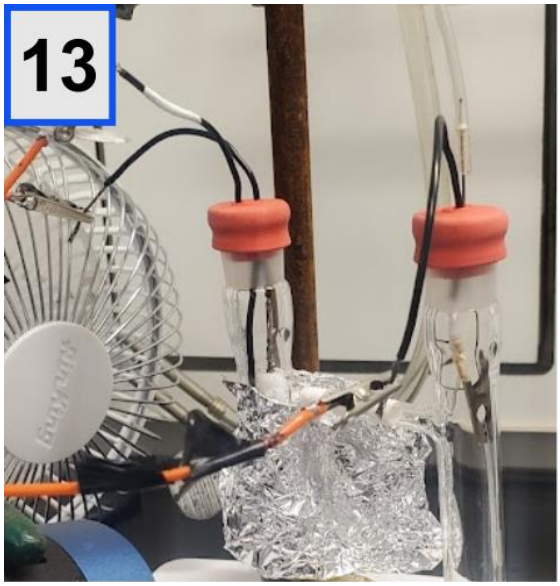

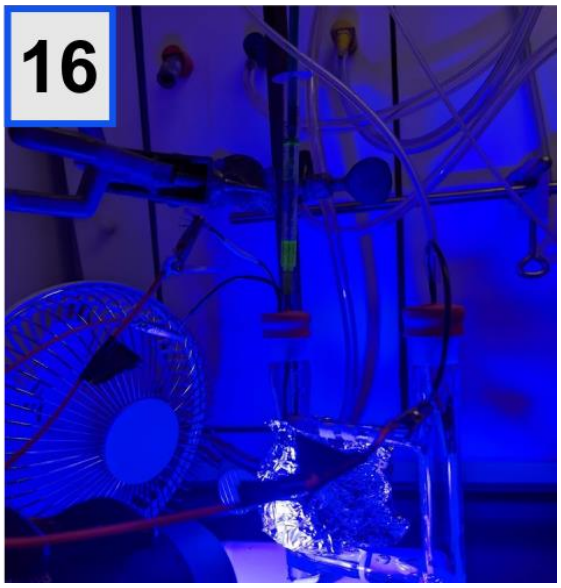

13. Attach electrode leads to working, reference, and counter electrode wires.
14. Apply a potential of −0.15 V vs SCE and irradiate reaction (440 nm).
15. After ~1 hour (when current has decreased ~75%), in a glovebox, dissolve the second catalyst portion in ~0.3 mL of 0.2 M $LiNTf_2$ in DME and transfer it to a syringe.
16. Remove the syringe from the glovebox and add the catalyst solution to the working electrode compartment.

A.11 Controlled potential coulometry traces

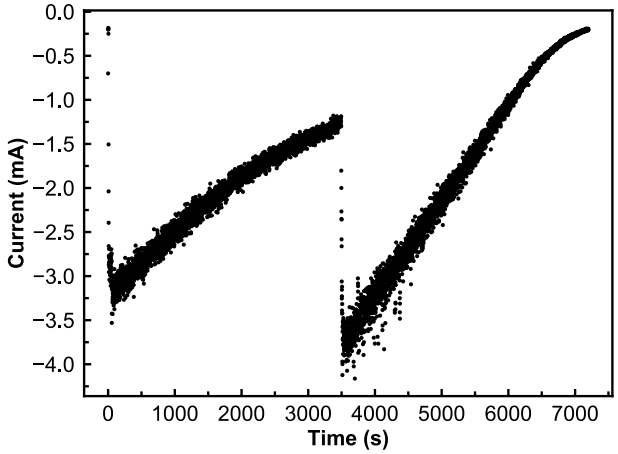

Figure A24. Current trace for a representative catalytic controlled potential coulometry experiment. Notice the increase in current in the first 5 seconds; the light is turned on after 5 seconds. At ~3600 seconds, the second portion of [Cu_2] is added, and an increase in current is observed.

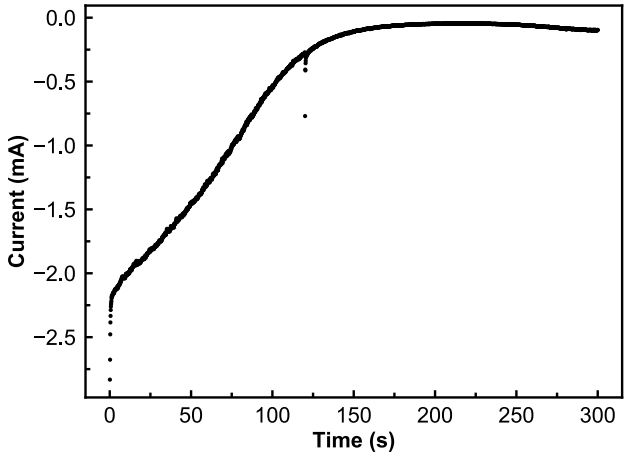

Figure A25. Current trace for the catalyst regeneration experiment described in the main text. After irradiating (440 nm) a solution of [Cu_2] and 4-methylbenzyl chloride in DME containing 0.2 M $LiNTf_2$ for 5 minutes, the solution was reduced at a carbon cloth electrode at −0.15 V vs SCE. The charge passed corresponds to 0.8 e^- per [Cu_2] equivalent.

A.12 Open circuit potential during irradiation

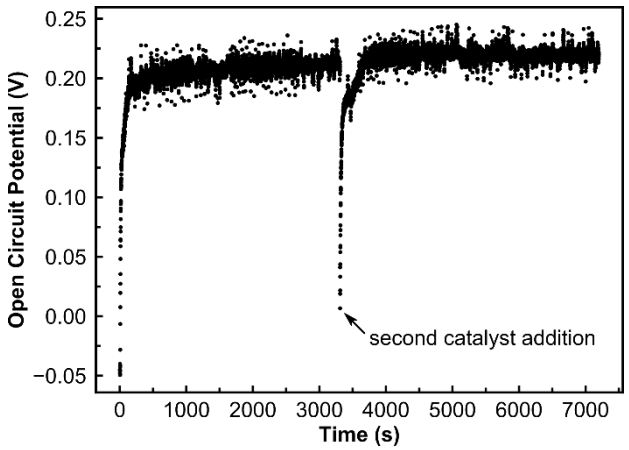

Figure A26. Open circuit potential (OCP) measurement for the control experiment in which no potential was applied in the presence of both catalyst and light (Scheme 5, Entry 4). Notice that the effective reaction rate can be intuited from the rapid decrease in OCP over the period of ~150 s at time = 0 s and time ~ 3200 s, corresponding to the beginning of the reaction and the addition of a second [Cu_2] catalyst portion, respectively.

A.13 Speciation after controlled potential coulometry

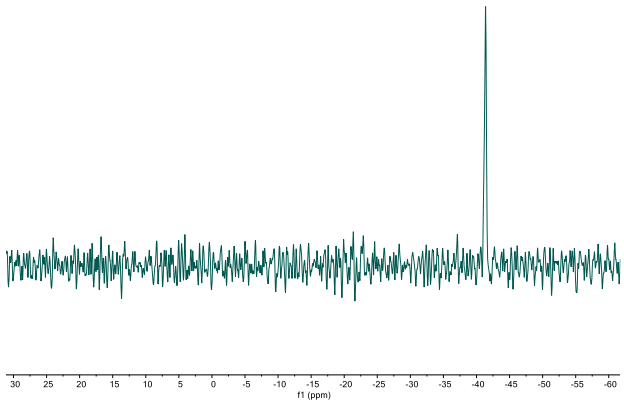

Figure A27. ^{31}P NMR spectrum of a crude reaction mixture post controlled potential coulometry. The reaction mixture was transferred from the two-compartment electrochemical cell into an NMR tube using inert-atmosphere syringe techniques. The chemical shift is that of chloro-diamond.

A.14 qNMR yields and isolated NMR spectra for catalytic experiments

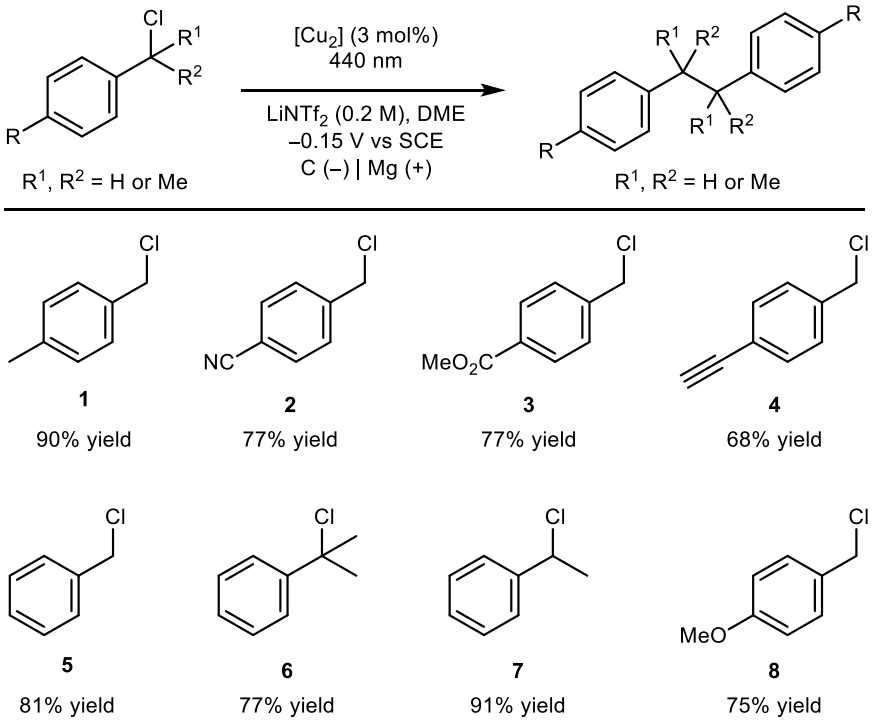

Figure A28. Electro-photocatalytic reduction of substituted benzyl chlorides featuring various substituents. NMR yields for the average of two runs are reported.

References for reported NMR characterization data

Substrates	Ref
1, 2, 5, 7	9
3, 8	10
6	11
4	12

1-D (1,2-di-*p*-tolylethane)

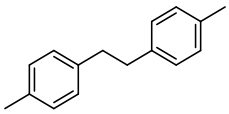

The general procedure from A.10 was used, employing 4-methylbenzyl chloride (21.1 mg, 0.15 mmol) as the electrophile. The reaction was worked up after 2 hours (89% NMR yield, 90% FE) and purified via column chromatography using ethyl acetate:hexane (0:1 to 1:100) as eluant to afford the product as a white solid (14.4 mg, 91%). TLC plates were visualized with ceric ammonium molybdate (blue spot; hexane, R_f = 0.4). Spectroscopic data was consistent with reported data.[9]

^{1}H NMR (qNMR left, isolated right):

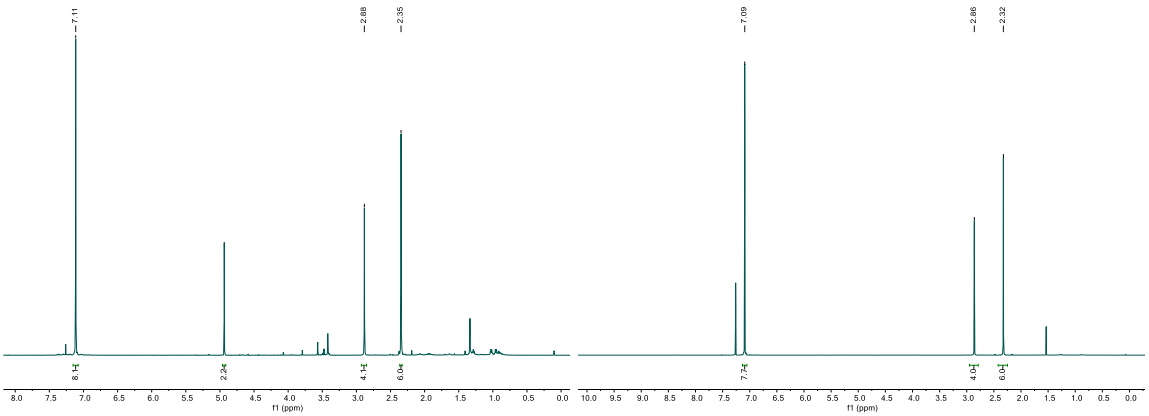

^{13}C{^{1}H} NMR:

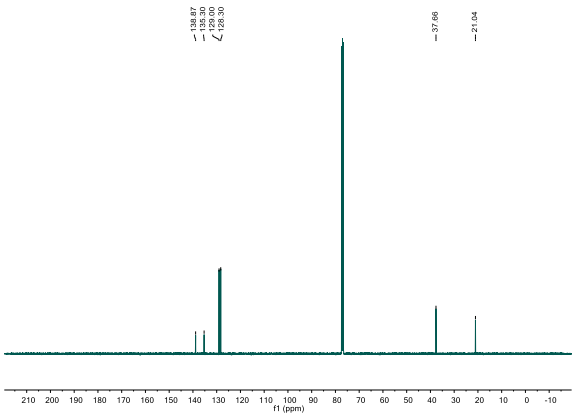

2-D (4,4'-(ethane-1,2-diyl)dibenzonitrile)

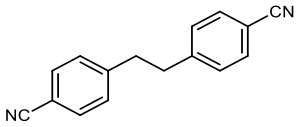

The general procedure from A.10 was used, employing 4-cyanobenzyl chloride (22.7 mg, 0.15 mmol) as the electrophile. The reaction was worked up after 1.5 hours (74% NMR yield, 78% FE) and purified via column chromatography using dichloromethane as eluant to afford the product as a white solid (12.7 mg, 74%). TLC plates were visualized by UV (dichloromethane, R_f = 0.4). Spectroscopic data was consistent with reported data.[9]

^{1}H NMR (qNMR left, isolated right):

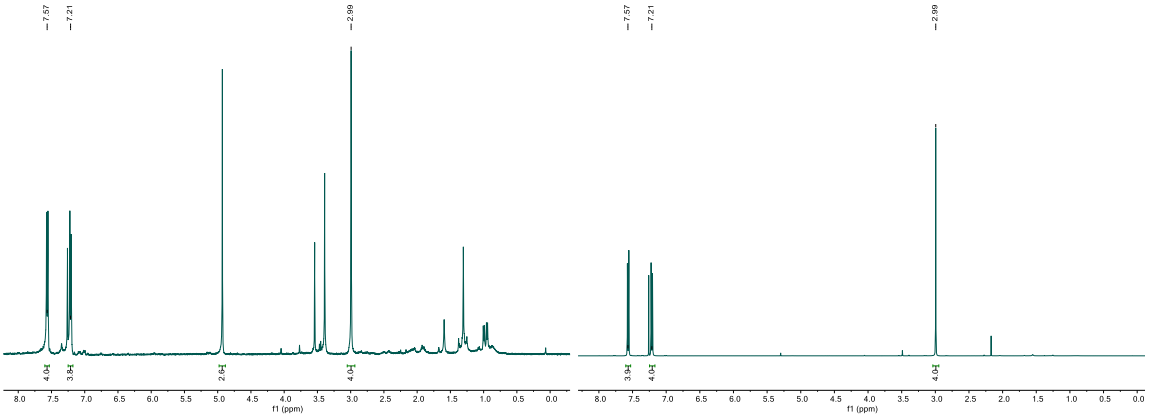

^{13}C{^{1}H} NMR:

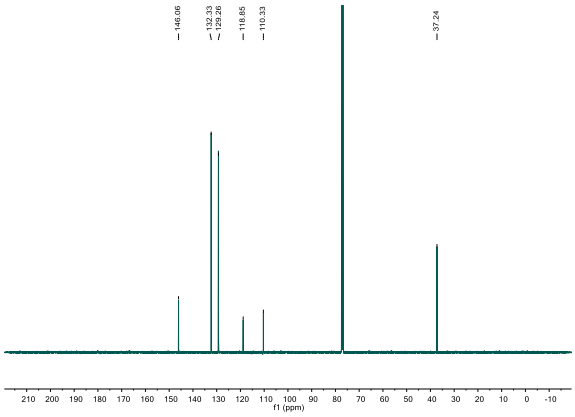

3-D (dimethyl 4,4'-(ethane-1,2-diyl)dibenzoate)

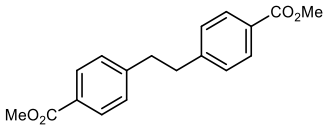

The general procedure from A.10 was used, employing methyl 4-(chloromethyl)benzoate (27.7 mg, 0.15 mmol) as the electrophile. The reaction was worked up after 2.5 hours (76% NMR yield, 78% FE) and purified via column chromatography using ethyl acetate:hexane (1:9 to 1:4) as eluant to afford the product as a white solid (16.5 mg, 74%). TLC plates were visualized by UV (ethyl acetate:hexane (1:9), R_f = 0.2). Spectroscopic data was consistent with reported data.[10]

^{1}H NMR (qNMR left, isolated right):

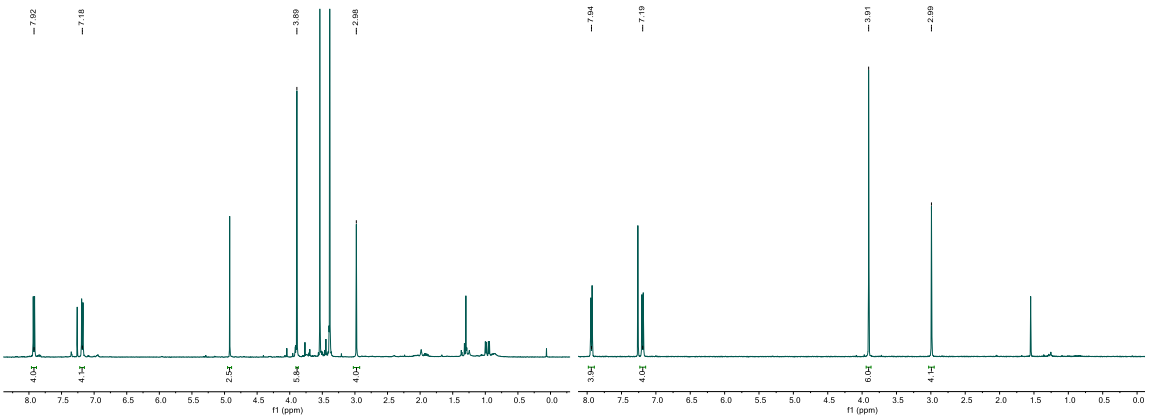

^{13}C{^{1}H} NMR:

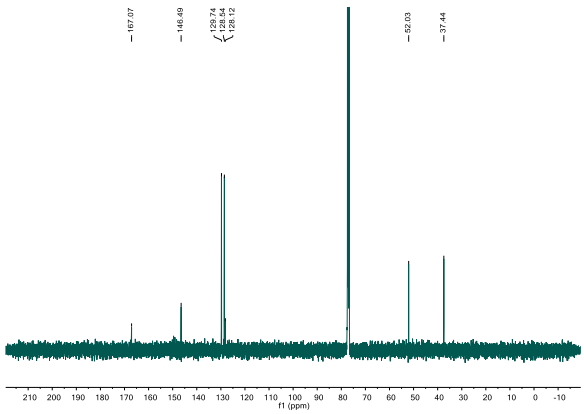

4-D (1,2-bis(4-ethynylphenyl)ethane)

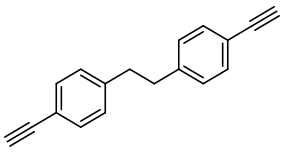

The general procedure from A.10 was used, employing 1-(chloromethyl)-4-ethynylbenzene (22.6 mg, 0.15 mmol) as the electrophile. The reaction was worked up after 1.5 hours (73% NMR yield, 77% FE) and purified via column chromatography using ethyl acetate:hexane (2:98) as eluant to afford the product as a white solid (12.6 mg, 73%). TLC plates were visualized by UV (ethyl acetate:hexane (2:98), R_f = 0.4). Spectroscopic data was consistent with reported data.[12]

^{1}H NMR (qNMR left, isolated right):

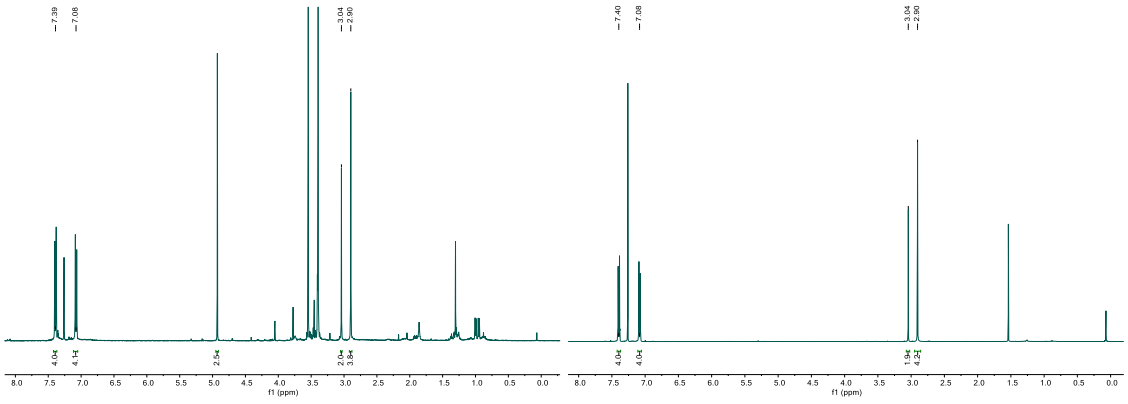

^{13}C{^{1}H} NMR:

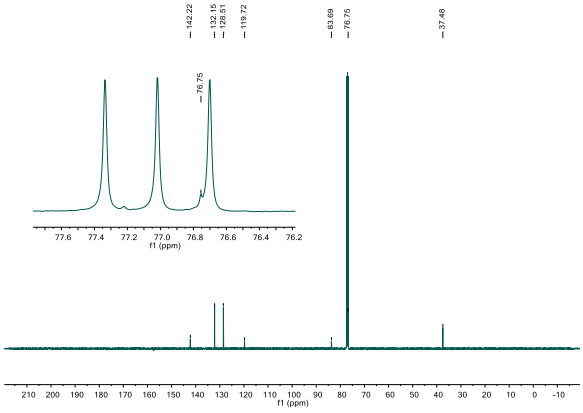

5-D (1,2-diphenylethane)

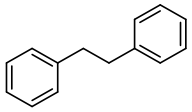

The general procedure from A.10 was used, employing benzyl chloride (19.0 mg, 0.15 mmol) as the electrophile. The reaction was worked up after 2 hours (82% NMR yield, 84% FE) and purified via column chromatography using ethyl acetate:hexane (0:1 to 1:100) as eluant to afford the product as a white solid (11.0 mg, 80%). TLC plates were visualized with ceric ammonium molybdate (blue spot; hexane, R_f = 0.4). Spectroscopic data was consistent with reported data.[9]

^{1}H NMR (qNMR left, isolated right):

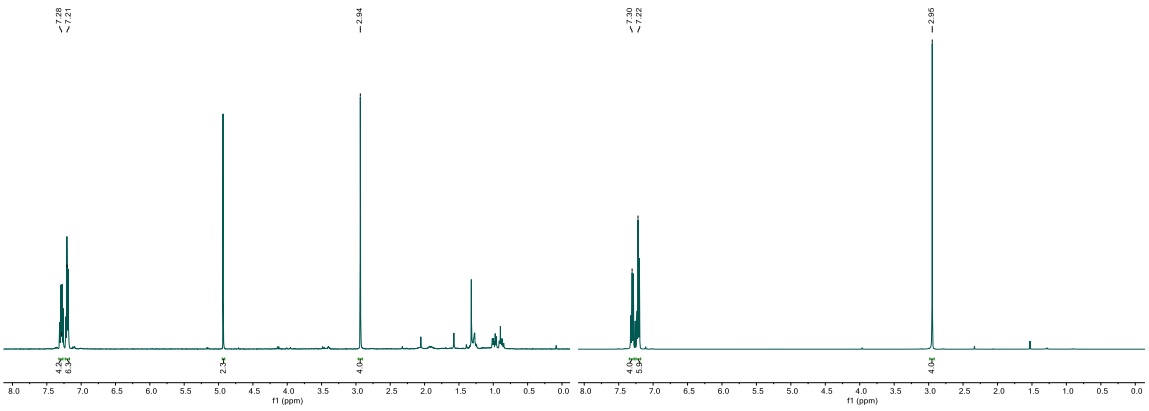

^{13}C{^{1}H} NMR:

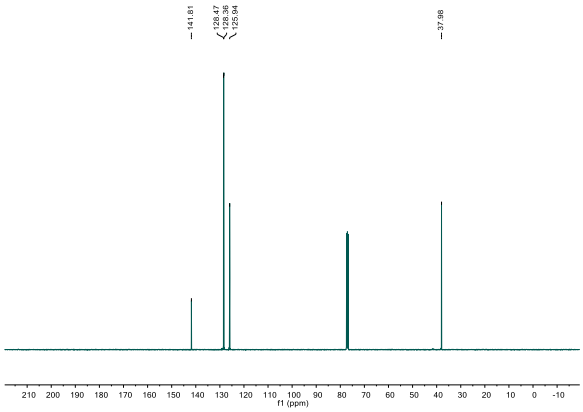

6-D (2,3-dimethyl-2,3-diphenylbutane)

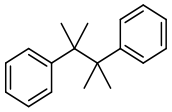

The general procedure from A.10 was used, employing (1-chloro-1-methylethyl)benzene (23.2 mg, 0.15 mmol) as the electrophile. The reaction was worked up after 1.5 hours (79% NMR yield, 99% FE) and purified via column chromatography using hexane as eluant to afford the product as a white solid (15.5 mg, 87%). TLC plates were visualized with ceric ammonium molybdate (blue spot; hexane, R_f = 0.4). Spectroscopic data was consistent with reported data.[13]

^{1}H NMR (qNMR left, isolated right):

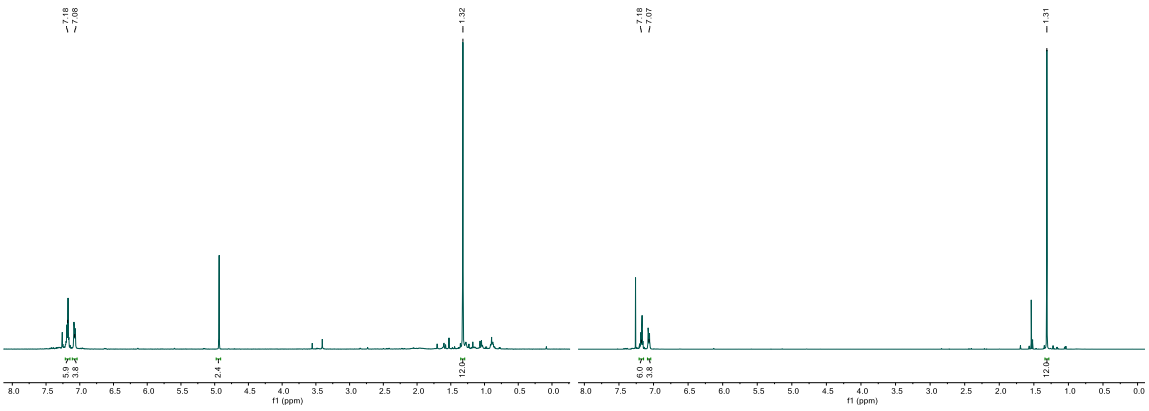

^{13}C{^{1}H} NMR:

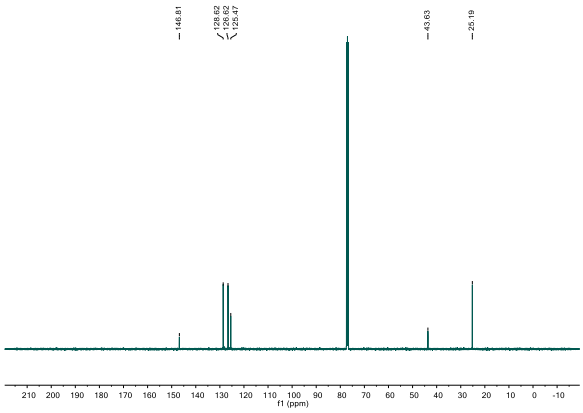

7-D (2,3-diphenylbutane)

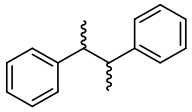

The general procedure from A.10 was used, employing (1-chloroethyl)benzene (21.1 mg, 0.15 mmol) as the electrophile. The reaction was worked up after 2 hours (92% NMR yield, 96% FE) and purified via column chromatography using hexane as eluant to afford the product as a white solid (12.2 mg, 77%). The product was isolated as an approximately equimolar mixture of diastereomers. TLC plates were visualized with ceric ammonium molybdate (blue spot; hexane, R_f = 0.4). Spectroscopic data was consistent with reported data.[9]

^{1}H NMR (qNMR left, isolated right):

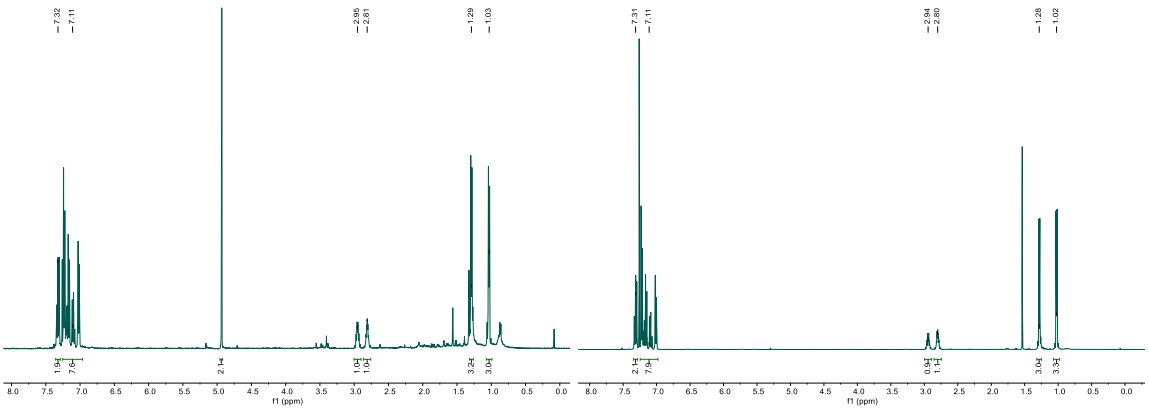

^{13}C{^{1}H} NMR:

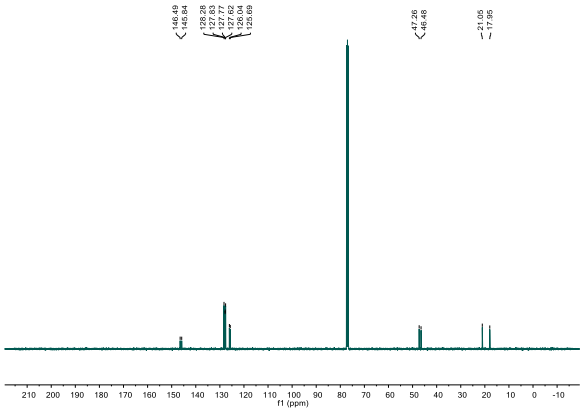

8-D (1,2-bis(4-methoxyphenyl)ethane)

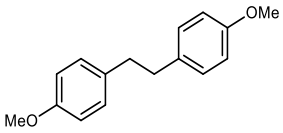

The general procedure from A.10 was used, employing 4-methoxybenzyl chloride (23.5 mg, 0.15 mmol) as the electrophile. The reaction was worked up after 2.5 hours (79% NMR yield, 93% FE) and purified via column chromatography using ethyl acetate:hexane (1:20) as eluant to afford the product as a white solid (14.3 mg, 79%). TLC plates were visualized with ceric ammonium molybdate (blue spot; ethyl acetate:hexane (1:20)), $R_f = 0.3$). Spectroscopic data was consistent with reported data.[10]

^{1}H NMR (qNMR left, isolated right):

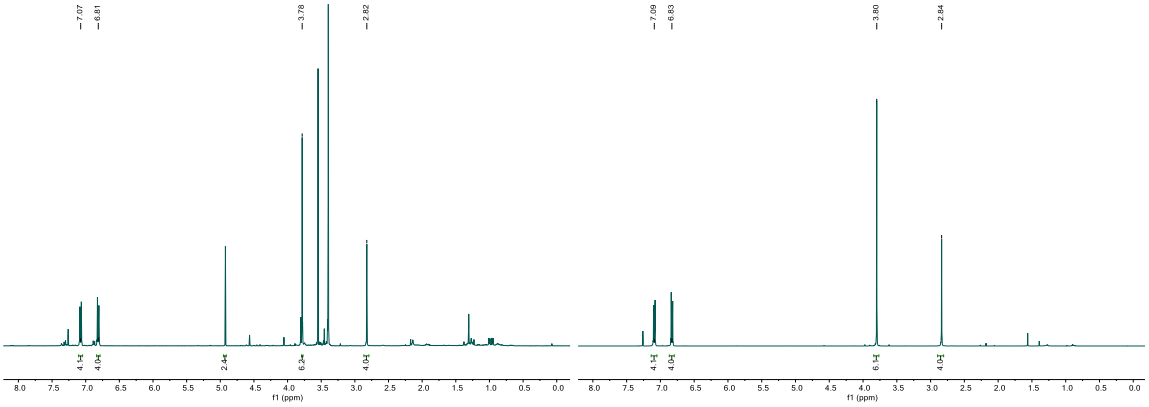

^{13}C{^{1}H} NMR:

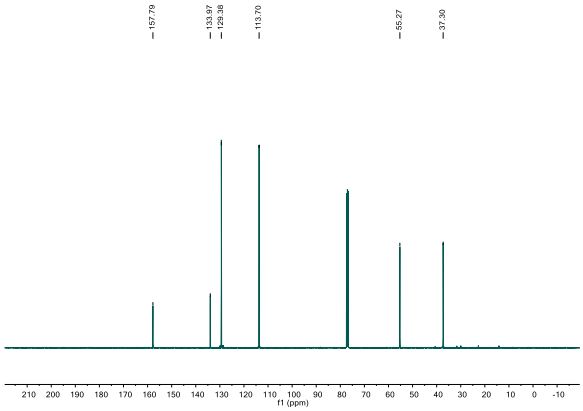

A.15 Synthesis and characterization of known electrophiles

1-(chloromethyl)-4-ethynylbenzene

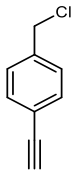

This compound was made by following a literature procedure,[14] and its spectroscopic data is consistent with reported data.[15]

^{1}H NMR:

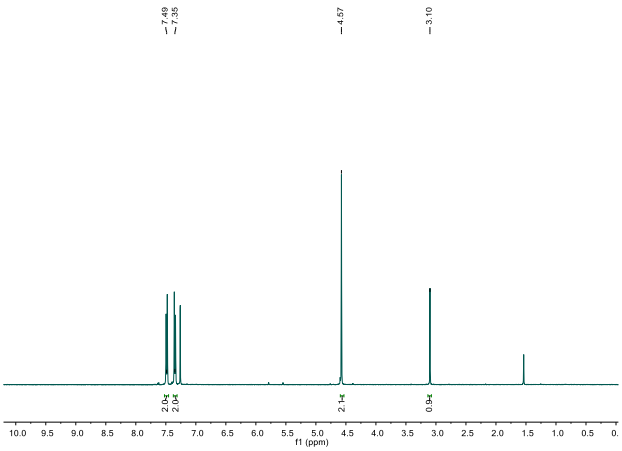

^{13}C{^{1}H} NMR:

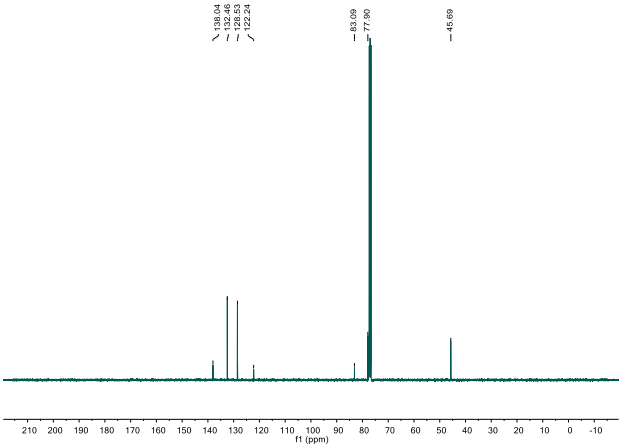

2-chloro-2-phenylpropane

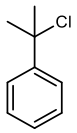

This compound was made by following a literature procedure, and its spectroscopic data is consistent with reported data.[16]

^{1}H NMR:

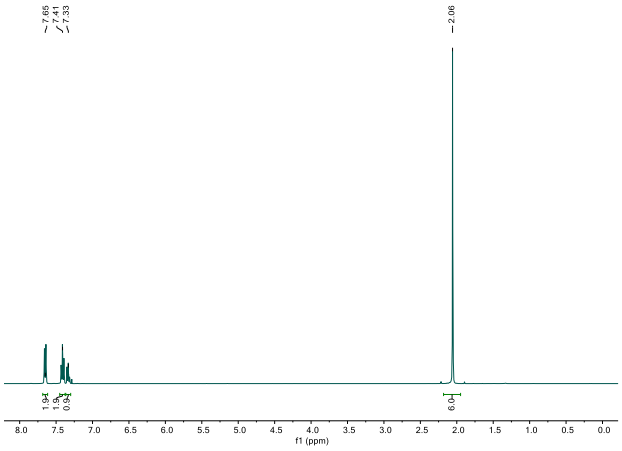

^{13}C{^{1}H} NMR:

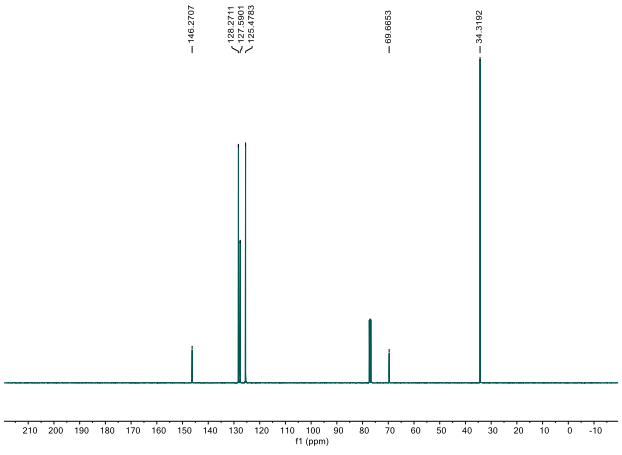

A.16 References

[1] Harkins, S. B.; Mankad, N. P.; Miller, A. J. M.; Szilagyi, R. K.; Peters, J. C. Probing the Electronic Structures of $[Cu_2(\mu\text{-}XR_2)]^{n+}$ Diamond Cores as a Function of the Bridging X Atom (X = N or P) and Charge (*n* = 0, 1, 2). *J. Am. Chem. Soc.* **2008**, *130*, 3478–3485.

[2] Connelly, N. G.; Geiger, W. E. Chemical Redox Agents for Organometallic Chemistry. *Chem. Rev.* **1996**, *96*, 877-910.

[3] Sheldrick, G. SHELXT - Integrated Space-Group and Crystal-Structure Determination. *Acta Crystallogr., Sect. C: Struct.* **2015**, *71*, 3–8.

[4] Dolomanov, O. V.; Bourhis, L. J.; Gildea, R. J.; Howard, J. A. K.; Puschmann, H. OLEX2: a Complete Structure Solution, Refinement and Analysis Program. *J. Appl. Crystallogr.* **2009**, *42*, 339–341.

[5] Eberson, L. *Electron-Transfer Reactions in Organic Chemistry*; Springer-Verlag: Berlin, 1987; p 32.

[6] Rehm, D.; Weller, A. Kinetics of Fluorescence Quenching by Electron and H-Atom Transfer. *Israel J. Chem.* **1970**, *8*, 259–271.

[7] Spek, A. L. Structure Validation in Chemical Crystallography. *Acta Cryst.* **2009**, *D65*, 148–155.

[8] Van der Sluis, P.; Spek, A. L. BYPASS: An Effective Method for the Refinement of Crystal Structures Containing Disordered Solvent Regions. *Acta Cryst.* **1990**, *A46*, 194–201.

[9] Sato, K.; Inoue, Y.; Mori, T.; Sakaue, A.; Tarui, A.; Omote, M.; Kumadaki, I.; Ando, A. Csp^3–Csp^3 Homocoupling Reaction of Benzyl Halides Catalyzed by Rhodium. *Org. Lett.* **2014**, *16*, 3756–3759.

[10] Cao, D.; Li, C.-C.; Zeng, H.; Peng, Y.; Li, C.-J. $C(sp^3)$−$C(sp^3)$ Bond Formation via Nickel-Catalyzed Deoxygenative Homo-Coupling of Aldehydes/Ketones Mediated by Hydrazine. *Nat. Commun.* **2021**, *12*, 3729.

[11] Z.-J. Wang, J.-J. Lv, R.-N. Yi, M. Xiao, J.-J. Feng, Z.-W. Liang, A.-J. Wang, X. Xu. Nondirecting Group sp^3 C−H Activation for Synthesis of Bibenzyls via Homo-coupling as Catalyzed by Reduced Graphene Oxide Supported PtPd@Pt Porous Nanospheres. *Adv. Synth. Catal.* **2018**, *360*, 932–941.

[12] Galán, E.; Perrin, M. L.; Lutz, M.; van der Zant, H. S. J.; Grozema, F. C.; Eelkema, R. Synthesis of 1,2-Biphenylethane Based Single-Molecule Diodes. Org. Biomol. Chem., **2016**, **14**, 2439–2443.

[13] Z.-J. Wang, J.-J. Lv, R.-N. Yi, M. Xiao, J.-J. Feng, Z.-W. Liang, A.-J. Wang, X. Xu. Nondirecting Group sp^3 C−H Activation for Synthesis of Bibenzyls via Homo-coupling as Catalyzed by Reduced Graphene Oxide Supported PtPd@Pt Porous Nanospheres. *Adv. Synth. Catal.* **2018**, *360*, 932–941.

[14] Landgrebe, J. A.; Rynbrandt, R. H. Synthesis and Solvolysis of o-, m-, and p-Ethynylbenzyl Chloride and Closely Related Structures. The Electronic Nature of the Acetylene Group. *J. Org. Chem.* **1966**, *31*, 2585–2593.

[15] Pedersen, P. J.; Henriksen, J.; Gotfredsen, C. H.; Clausen, M. H. Regio- and Stereoselective Hydrosilylation of Immobilized Terminal Alkynes. *Tetrahedron Lett.* **2008**, *49*, 6220–6223.

[16] Ajvazi, N.; Stavber, S. Direct Halogenation of Alcohols with Halosilanes Under Catalyst- and Organic Solvent-Free Reaction Conditions. *Tetrahedron Lett.* **2016**, *57*, 2430–2433.